Fine tuning of Piezo1 Expression and Activity Ensures Efficient Myoblast Fusion during Skeletal Myogenesis

Huascar Pedro Ortuste Quiroga[1*], Massimo Ganassi[3], Shingo Yokoyama[2], Kodai Nakamura[1], Tomohiro Yamashita[1], Daniel Raimbach[4], Arisa Hagiwara[1], Oscar Harrington[4], Jodie Breach-Teji[4], Atsushi Asakura[5], Yoshiro Suzuki[6], Makoto Tominaga[6], Peter S. Zammit[3], Katsumasa Goto[1,2,*]

[1] Department of Physiology, Graduate School of Health Sciences, Toyohashi SOZO University
[2] Laboratory of Physiology, School of Health Sciences, Toyohashi SOZO University
[3] Randall Centre for Cell and Molecular Biophysics, King's College London, London, SE1 1UL, UK
[4] Centre of Human and Aerospace Physiological Sciences, King's College London, London, SE1 1UL, UK
[5] Stem Cell Institute, Paul & Sheila Wellstone Muscular Dystrophy Center, Department of Neurology, University of Minnesota Medical School
[6] Division of Cell Signalling, National Institute for Physiological Sciences

* Correspondence: gotok@sepia.ocn.ne.jp, s1855105@sc.sozo.ac.jp

Abstract: Mechanical stimuli such as stretch and resistance training are essential to regulate growth and function of skeletal muscle. However, the molecular mechanisms involved in sensing mechanical stress during muscle formation remain unclear. Here, we investigate the role of the mechanosensitive ion channel Piezo1 during myogenic progression. Direct manipulation of Piezo1 in muscle stem cells alters their myogenic progression. Indeed, *Piezo1* knockdown suppresses myoblast fusion leading to smaller myotubes. Such event is accompanied by significant downregulation of the fusogenic protein *Myomaker*. In parallel, while *Piezo1* knockdown also lowers Ca^{2+} influx in response to stretch, Piezo1 activation increases Ca^{2+} influx in response to stretch and enhances myoblasts fusion. We believe these findings may help understand molecular defects present in some muscle diseases. Altogether our study shows that Piezo1 is essential for terminal muscle differentiation acting on myoblast fusion, suggesting that Piezo1 deregulation may have implications in muscle aging and degenerative diseases including muscular dystrophies.

Key words: skeletal muscle, satellite cells, mechanosensation, Piezo1, Ca^{2+} channel, myocyte fusion

1. Introduction

Skeletal muscle is a highly specialised tissue composed of multi-nucleated, post-mitotic myofibres. Since myonuclei within a myofibre do not divide after development, the production of new myonuclei, to sustain muscle maturation and repair, is entrusted to muscle stem cells (named satellite cells (SCs)). SCs are found on the surface/periphery of postnatal skeletal myofibres [1-3] and in response to muscle damage or hypertrophic stimuli, rapidly activate to generate a myoblast progeny that proliferate, undergo myogenic differentiation, and finally fuse to repair damaged myofibres, resulting in regeneration of a functional muscle [4]. Therefore, alterations in the myoblast fusion machinery can have profound effects on regeneration efficiency. An important process dictating myoblast fusion is mechanosensation, but how this is regulated in muscle remains largely unknown.

Mechanosensitive (MS) ion channels are pore-forming membrane proteins which gate in response to mechanical stimuli applied on the cell membrane [5-7]. MS ion channels have been linked to many physiological processes associated with mechanosensory transduction; including osmoregulation, proprioception, hearing, touch, blood flow regulation to name but a few examples [8-10]. Piezo1 and Piezo2 were first identified as the long-sought principal types of molecular force sensors (mechanosensors) in mammalian

cells [5]. Piezo1, and similarly Piezo2, are very large proteins containing ~2500 amino acids with each subunit (three subunits per channel) having an estimated 24-40 transmembrane (TM) segments [6, 8, 11, 12]. Characterisation of ionic selectivity revealed that Piezo1 was nonselective, permeating Na^+, K^+, Ca^{2+} and Mg^{2+} with a preference for Ca^{2+} [5, 13]. Ca^{2+} regulation plays a crucial role in skeletal muscle maintenance and repair, thus understanding Piezo1's function may prove vital when developing therapeutic interventions for muscular dystrophies [14, 15].

Here, we analyse the role of Piezo1 in skeletal myogenesis, focussing on muscle differentiation and its role in stretch-induced Ca^{2+} influx of primary myoblast-derived myotubes. Our findings reveal that *Piezo1* is dispensable for myoblast proliferation and onset of differentiation, but is finely regulated during myoblast fusion and myofibre maturation. Indeed, *Piezo1* knockdown suppresses myotube formation and maturation in primary myotubes derived from mouse slow soleus (SOL) and fast extensor digitorum longus (EDL) muscles. At the molecular level, *Piezo1* reduction leads to downregulation of the fusogenic gene *Myomaker*, decreases filamentous actin (f-actin) accumulation and organisation and lowers Ca^{2+} influx of myotubes in response to mechanical stretch. In contrast, administration of the Piezo1-specific agonist Yoda1 increased myoblast fusion. Congruently, Piezo1 activation also showed increased Ca^{2+} influx in response to stretch. In summary, we show that Piezo1 plays a crucial role at the terminal stage of myoblast myocyte fusion and myofibre maturation.

2. Materials and Methods

Primary myoblast cell culture

All experimental procedures were carried out in accordance with the Guide for the Care and Use of Laboratory Animals as adopted and promulgated by the National Institutes of Health (Bethesda, MD, USA) and were approved by the Animal Use Committee of Toyohashi SOZO University A2018006, A2019006). Male C57BL/6J mice (8-12 weeks of age) were used. All mice were housed in a vivarium room with 12-h-12-h light-dark cycle; with temperature and humidity maintained at ~23°C and ~50%, respectively. Solid food and water were provided *ad libitum*.

After cervical dislocation, the EDL (*extensor digitorum longus*) and SOL muscles were carefully dissected, and manipulated only by their tendons. Muscles were digested in 0.2% Collagenase Type 1 (Sigma, UK. Ref: SCR103) in Dulbecco's Modified Eagle Medium (DMEM, Gibco, Thermo Fisher Scientific, Ref: 11885084) with 1% penicillin/streptomycin (Pen Strep, Gibco, Thermo Fisher Scientific, Ref: 15140-122) for 2 hours. Individual myofibres were then dissociated by trituration using heat polished glass Pasteur pipettes (Marienfeld, Germany. Ref: 3233049) with variously sized apertures (coated with 5% BSA, Sigma-Aldrich, Ref: A7906-100G) and washed as described by Collins and Zammit (2009)[16]. Isolated myofibres were plated on Matrigel (Corning. Ref: 354234) and the SC-derived myoblasts were then expanded in proliferation medium, consisting of; DMEM, with 30% heat-inactivated foetal bovine serum (FBS) (Gibco, Thermo Fisher Scientific. Ref: 26140-079), 10% horse serum (Gibco, Thermo Fisher Scientific, Ref: 16050-122), 1% chick embryo extract (Sera Laboratories. Ref: CE-650-TL), 10 ng/ml basic FGF (bFGF, Gibco, Thermo Fisher Scientific. Ref: PHG0264) and 1% penicillin. Cells were kept in a 37°C incubator (Panasonic, MCO-230AICUVH) under a humidified atmosphere with 95% air and 5% CO_2. Cells designated for proliferation and differentiation conditions were seeded at different densities depending on the size of wells they were cultured in. For 96-well plate proliferation conditions required 5,000 cells per well, and for differentiation, cells were seeded at 10,000 cells per well. For 6-well plates, proliferating and differentiation cohorts consisted of 50,000 cells and 70-80,000 per well, respectively. Differentiation medium was made up of DMEM, 2% heat-inactivated horse serum, and 1% penicillin.

siRNA transfection

Small interfering RNAs (siRNAs) were purchased from (Qiagen, Hiden, Germany) (Table 1) and diluted to 20 or 10 μM in double-distilled water (ddH2O) and stored at -20°C. To investigate the effects *Piezo1* knockdown on proliferation, early entry into differentiation and myotube formation, *Piezo1*-targeting or control scrambled siRNA (siScrambled; Qiagen, Hiden, Germany) was transfected in proliferation medium. Cells were plated on 6-well plates at 50,000 cells per well in proliferation medium. Following a 24 h incubation period, the medium was replaced with 1.75 ml fresh proliferation medium and the transfection mixture was prepared: A solution 150 μl Optimem (Gibco, Thermo Fisher Scientific. Ref: 31985-070) medium with 9 μl of lipofectamine (lipofectamine RNAiMAX Thermo Fisher Scientific. Ref: 13778030) was made for each well. Separately, siRNA was diluted in 150 μl Optimem. The two solutions were then mixed and incubated for 5 min. 250 μl of the siRNA/lipofectamine mixture was added to corresponding wells dropwise. The final siRNA concentration was set at 10 nM. Following overnight incubation in the transfection medium, cells were trypsinised for RT-qPCR analysis and seeded in 96-well plates for proliferation and differentiation cohorts (day 1 and day 3 differentiation) in proliferation and differentiation medium, respectively. After a 24-hour incubation, proliferating cells were subjected to a 2-hour 5-ethynyl-2'-deoxyuridine (EdU) pulse and fixed as below. Day 1 and day 3 differentiating cohorts were also fixed.

To determine *Piezo1*'s role in myotube formation, siRNA transfection was performed in early differentiated myotubes. Cells were seeded at confluency in differentiation medium. Following 24-hour incubation in differentiation medium, siRNA transfection was performed. Cohorts were designated for RT-qPCR analyses and immunolabelling.

Table 1. List of siRNAs used

Gene	Species	siRNA ID
scrambled non-targeting siRNA (All Stars Negative Control siRNA)	Mouse	Qiagen, 1027281
Piezo1	**Mouse**	**Qiagen, S104420409**
Piezo1	Mouse	Qiagen, S104420402
Piezo1	Mouse	Qiagen, S100814807
Piezo1	Mouse	Qiagen, S100814821

N.B. The highlighted *Piezo1* siRNA (S1044120409) was used for most of the experiments. The other three were used as validators of our obtained results.

RNA Extraction and Reverse Transcription

RNA was extracted from cells using the RNeasy mini kit as per manufacturer's requirements (Qiagen. Ref: 217004). Reverse transcription was carried out using PrimeScript RT Master Mix (Takara Bio, Otsu, Japan. Ref: RR036A). Optical density analysis using a Nanodrop ND-1000 spectrophotometer (Labtech, UK) quantified RNA concentration. Samples were then loaded to a PCR thermal cycler (Takara, Dicemini). The resulting cDNA was then diluted 1:9 to obtain a working dilution for RT-qPCR analysis.

Real-time Quantitative PCR (RT-qPCR)

Primers were designed using the Takara Bio Perfect Real Time Support System (Takara Bio, Table 2). Primers were diluted to 50 µM in ddH_20 and stored at -20°C. Real-time RT-qPCR was performed on the cDNA (Thermal Cycler Dice Real Time System IIMRQ, Takara Bio) using Takara SYBR Premix Ex Taq II (Takara Bio. Ref: RR802A). 12.5 µl of SYBR Premix Ex were added to each RT-qPCR well. 8.5 µl of ddH20 and 2 µl of the corresponding primers were then added (a final concentration of 2 µM per primer). 2 µl of the respective cDNA was then added to the appropriate wells, bringing the total volume to 25µl per well. The RT-qPCR cycle consisted of 95°C for 30 s (for enzyme activation), followed by 40 cycles at 95°C for 5 s and a qPCR amplification period of 30 s at 60°C. The relative fold change of expression was calculated by the comparative threshold cycle (CT) method using Takara Thermal Cycler Dice Real Time System Software Ver. 4.00 (Takara Bio). To normalise for the amount of total RNA present in each reaction, *Gapdh* was used as an internal standard.

Table 2. RT-qPCR primers

Gene	Species	Forward primer (5'-3')	Reverse primer (5'-3')	Reference
Gapdh	Mouse	TGTGTCCGTGGATCTGA	TTGCTGTTGAAGTCGCAGGAG	Takara Bio, MA050371
Piezo1	Mouse	CTTTATCATGAAGTGCAGCCGAG	CCAGATGATGGCGATGAGGA	Takara Bio, MA125411
Myomaker	Mouse	CATGCGCCGTGACATTCTG	AAGCATTGTGAAGGTCGATCTCTG	Takara Bio, MA131293
Myomixer	Mouse	GAATCCACCGCAGGCAAA	ACCATCGGGAGCAATGGAAC	Takara Bio, MA101853

Piezo1 activation

In order to induce Piezo1 activation, early forming myotubes were subjected to the Piezo1 specific agonist Yoda1 (Cayman Chemical Company. Ref: 21904) diluted in dimethyl sulfoxide (DMSO, Sigma. Ref: D2650-5x5ML). This consisted of a 24-hour incubation period in differentiation medium at high confluency (10,000 cells/well). By this point myoblasts seeded at high confluency, begin to show myotube formation in the relatively small 96-well plates. These early formed myotubes were then administered Yoda1. Yoda1 binds the agonist transduction motif (ATM), located at the pore domain of the Piezo1 channel [17]. With each subunit displaying such motif, Yoda1 has potentially three binding sites. This phase of the investigation consisted of two main variables 1) drug

concentration and 2) duration of time cells were incubated with the drug. Five concentrations were chosen in order to cover an increasing spectrum of Yoda1 final concentration, these were: 5, 10, 30 and 100 μM diluted in differentiation medium. Preliminary findings from the group found that a 24-hour incubation with any of the concentrations chosen, led to complete abolishment of myotube maturation (data not show). Thus, time-points thought to have potential to maximise myoblast fusion/myotube maturation were tested. The incubation time-points were set for 1 and 30 min, 1 and 4 hours. Control cohorts containing only DMSO were incubated at the allocated times to allow comparisons to be made within each condition. Following the incubation of Yoda1 or DMSO, cells were cultured in the differentiation medium for a further 2 days (i.e. myotubes were analysed 3 days post initial induction of differentiation).

Immunolabelling

Throughout the protocol, all washes were performed with Dulbecco's phosphate-buffered saline (DPBS, Gibco, Dulbecco's Phosphate Buffered Saline, Thermo Fisher Scientific, Ref: 14190-144). Cells were fixed with 4% paraformaldehyde for 15 min. Samples were then washed three times with PBS (5 minutes each wash) and permeabilised for 15 min using 0.5% triton-X100/PBS (Sigma-Aldrich. Ref: T9284-500ml). Cells were blocked for 1 hour in 5% bovine serum albumin (BSA, Sigma-Aldrich Ref: A7906-100G). Primary antibodies (diluted to the working concentration in PBS) (Table 3) were added to the samples and incubated overnight at 4^0C. Primary antibodies were decanted, the samples were washed three times and appropriate secondary antibodies diluted to the working concentration in PBS added (Table 3) were added to the samples. The samples were covered with aluminium foil to avoid light exposure and left to stand at room temperature for 1 hour. Cells were washed again (three times). To visualise nuclei, the cells were incubated for 10 min at room temperature with 1 μg/ml 4', 6-diamidino-2-phenylindole (DAPI) (Sigma. Ref: D9542-10MG) diluted 1:1000 in PBS. After a final wash with PBS (5 min), cells were replenished with PBS and stored at 4 ^{0}C until image analysis.

EdU incorporation

For the evaluation of cell proliferation, cells were incubated with 5-ehtynyl-2'-deoxyuridine (EdU: Invitrogen, Thermo Fisher Scientific) at 10 μM, added in fresh proliferation medium for 2 hours at 37 °C. EdU, the alkyne-containing thymidine analog, is incorporated into DNA during active DNA synthesis. The click-iT EdU Alexa Flour kit (Invitrogen, Thermo Fisher Scientific, Click-iT, EdU Alexa Fluor. Ref: 594 C10339) was used as per manufacturer's instructions with either the 488 (green) or 594 (red) azide to detect incorporated EdU.

Phalloidin labelling

To evaluate the cytoskeleton, cells were treated with phalloidin (Invitrogen, Thermo Fisher Scientific, Alexa-Fluor. Ref: 488 A12379) diluted 1:40 in PBS. Phalloidin binds to f-actin, a major cytoskeleton protein in myofibres. Cells were incubated with phalloidin solution for 30 mins at room temperature. Cells were then washed with PBS twice for 5 min.

Table 3. Primary and Secondary antibodies used

Primary antibody	Dilution	Reference
Monoclonal mouse – Myogenin	1:10	Development Studies Hybridoma Bank (DSHB), F5D-s
Monoclonal mouse – MF20 (Myosin Heavy Chain)	1:10	Development Studies Hybridoma Bank (DSHB), MF20-s
Secondary antibody	**Dilution**	**Reference**
Donkey anti-mouse IgG (H+L), Alexa Fluor® 555	1:500	Life Technologies, A21203

Image analysis and quantification

Images were taken using a fluorescence microscope (BZ-X710, KEYENCE, Osaka, Japan). Four to five images per each well (3 wells per repeat) consistent of a total of 12-15 images per repeat were analysed. One repeat refers to one mouse. For EdU incorporation, the total number of DAPI-counterstained nuclei and total number of EdU-incorporated cells were quantified. The proportion of EdU-incorporated cells relative the total number of nuclei was subsequently expressed as percentages. The relative proportion of cells expressing Myogenin was also quantified in this manner.

The fusion index was calculated by quantifying the total number of nuclei within MyHC-positive myotubes and expressing this value as a proportion of the total number of nuclei in each field of view. As a criterion, more than two nuclei must be within a MyHC-positive myotube to be quantified for the fusion index: (MyHC-positive myotubes containing ≥2 nuclei/total number of nuclei) × 100.

To measure myotube width, the "measure" tool on ImageJ imaging software was used. This allows measurements of a chosen distance to be made. Before measurement, a scale was applied to all images. On the "set scale" option pixels are converted into μm. Taking the fluorescence microscope and magnification into account the program determines 100 μm to be 133.00 pixels or 0.75 μm/pixel. Three independent images were chosen per condition. The criterion for this analysis was to choose the widest possible distance between myotube edges without the presence of any branching points. This was carried out in three independent points within the field of view. The values were then averaged.

Stretch experiments and imaging of intracellular Ca^{2+} level

Stretch experiments were performed at the National Institute for Physiological Sciences (NIPS). Myoblasts were seeded (30,000 cells/chamber) on modified elastic silicone chambers (Strexcell, Ooyodonaka, Ref: STB-CH-0.02). After 24-hour incubation, cells were transfected with either control (siScrambled) or *Piezo1*-specific siRNA in proliferation medium. After overnight incubation, cells were switched to differentiation medium and cultured for a further 3 days. Stretch experiments were conducted on the third day. For Piezo1 activation by Yoda1 administration, cells were seeded as above. Following the initial overnight incubation, cells were switched to differentiate and the resulting myotubes were analysed 3 days post differentiation induction.

For Ca^{2+} imaging, Fura 2-AM (Invitrogen) with 10% Pluronic® F-127 (Molecular Probes, USA) diluted in double distilled water (ddH_2O), was administered to EDL- and SOL-derived myotubes followed by a 30-min incubation time. Chambers were attached

to an extension device (modified version of STB-150, Strex) on the microscope stage. Stretch stimulation was applied using a pre-set stretch speed and distance. After an initial 1 min rest period (0% stretch), stretch was applied at 3% (0.3 mm), 6% (0.6 mm) and 9% (0.9 mm) for 1 min followed by a 1-min resting period in between. During the initial 0% stretch timepoint, Yoda1 cohorts were administered with 30 μM of the agonist before being subjected to stretch. Ionomycin (Sigma-Aldrich) at 5 μM was applied at the final step in each experiment for normalisation and to check cell viability.

Changes in intracellular calcium [Ca^{2+}]i were measured by ratiometric imaging with Fura 2-AM at 340 and 380 nm, and the emitted light signal was read at 510 nm. Images were then analysed on ImageJ imaging software. Three independent myotubes from each condition were selected and analysed. The changes in ratios were calculated by subtracting basal values from peak values. The values were then normalised to ionomycin data.

Statistical analysis

Data is presented as mean ± SEM from at least three experiments (at least three mice). Significance was assessed by either paired Student's t-test or one-way ANOVA followed by followed by the Tukey-Kramer post-hoc; wherein p-values of < 0.05 were considered to be statistically significant. A paired t-test was adopted when comparing effects within the same group e.g., analysing the effects of siRNA mediated down-regulation of *Piezo1* versus siRNA controls in murine derived myoblasts. A one-way ANOVA was implemented when two or more independent groups were analysed, for example; comparing the effects of varying agonist concentrations across different timepoints.

3. Results

3.1 Piezo1 is upregulated during myoblast differentiation

To investigate the expression level of *Piezo1* during myogenic progression we used murine fast EDL and slow SOL muscle SC-derived primary myoblasts (Figure 1a). The expression of EDL muscle SC-derived primary myoblasts showed a significant increase in mRNA expression of *Piezo1* in myotubes cultured at 3 days of differentiation, compared to the expression level in proliferating myoblasts (Figure 1b). In SOL-derived myoblasts, *Piezo1* expression rapidly increased after 24 h, suggesting an earlier function of Piezo1 in slow muscle myogenesis. Indeed, *Piezo1* was found upregulated at both 24 h (4-fold) and 72 h of differentiation SOL-derived myoblasts compared to EDL-derived myoblasts (Figure 1b) where *Piezo1* increased by 2-fold. Thus, *Piezo1* expression increases during myoblast differentiation.

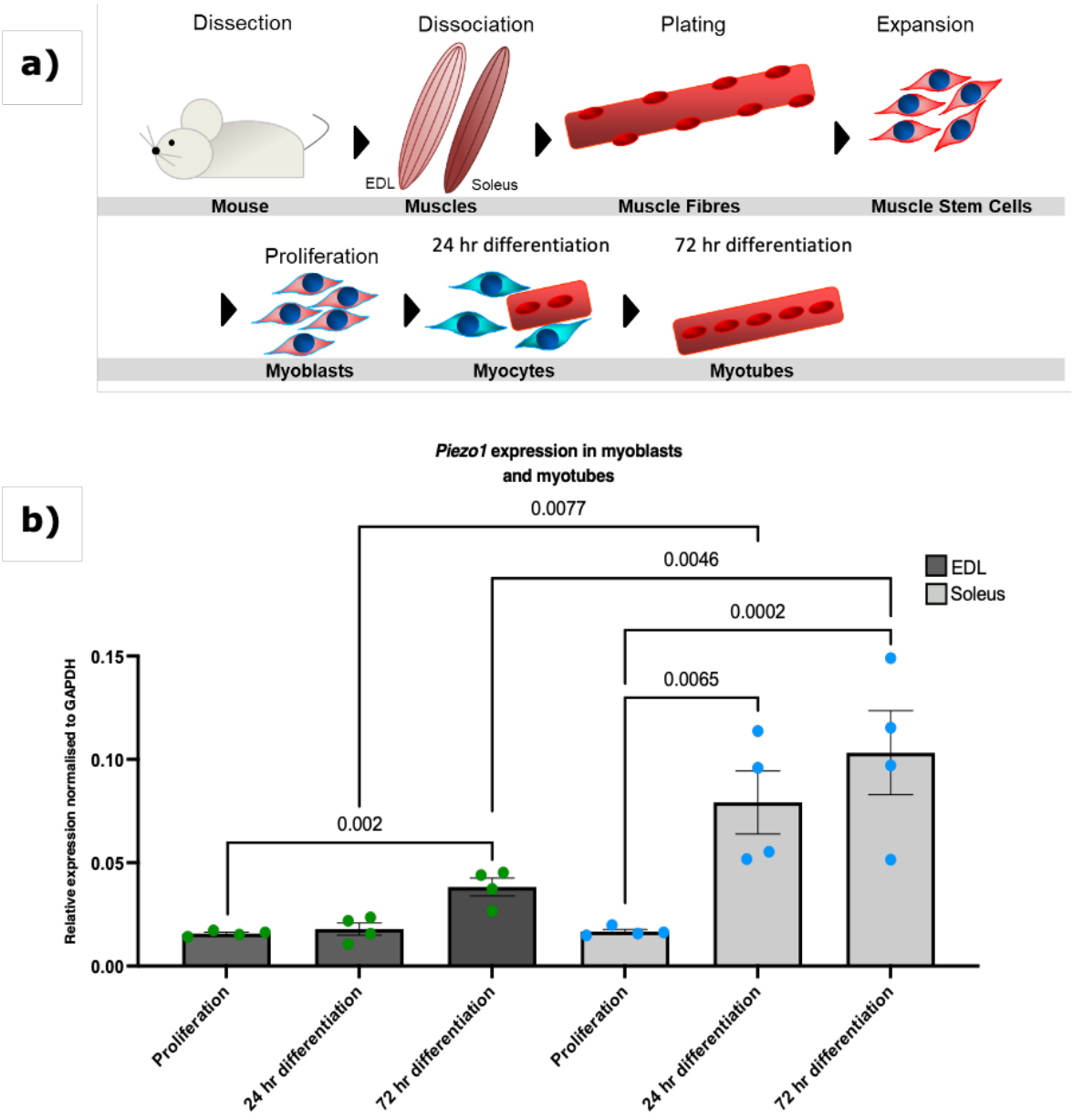

Figure 1. *Piezo1* expression increases in differentiating SC-derived myoblast. (**a**) Schematic representation of muscle isolation and SC-derived myoblast expansion procedure. (**b**) Relative fold changes in expression of *Piezo1* in myoblasts from EDL (dark grey bars, green dots) and SOL muscle (light grey bars, blue dots), during proliferation and through differentiation; 24 hours (Day 1) and 72 hours (Day 3) in differentiation medium. Values were normalised to *Gapdh*. Data is presented as mean ± SEM from four experiments (n = 4 mice). p values are annotated above graphs.

3.2 Piezo1 regulates Ca^{2+} influx during myogenesis

The Piezo1 channel permeates Ca^{2+} influx at a greater preference than other cations (Na^{+}, K^{+} and Mg^{2+}) [5]. Ca^{2+} is itself a crucial regulatory of muscle contraction and earlier during muscle formation and differentiation/fusion [18-20]. Thus, given accumulation of *Piezo1* mRNA in differentiating myoblasts, we sought to assess the dynamics of Ca^{2+} influx ($[Ca^{2+}]i$) upon modulation of Piezo1 activity in cultured myotubes. Using the customised stretch silicon bio-chambers [21], we cultured myotubes derived from both EDL- and SOL-derived myoblasts. We then divided the samples into two groups; those administered *Piezo1* specific siRNA (*Piezo1*-knockdown) and those given the Piezo1 agonist Yoda1 (at 30 μM). Results were compared against their respective controls (no Yoda1 or siRNA controls). The chambers were subjected to incremental bouts of stretch, with a minute rest in between each stretch. Throughout the experiment we measured $[Ca^{2+}]i$ (Figure 2). *Piezo1* siRNA-mediated knockdown led to nearly 50% and 40% reduction on *Piezo1* mRNA in EDL-derived myoblasts (Supplementary Figure 1a) and SOL-derived myoblasts (Supplementary Figure 1b) respectively, compared to control conditions. Under control conditions (siRNA controls and no Yoda1), upon mechanical stretch, $[Ca^{2+}]i$ increases significantly in both EDL-derived and SOL-derived myotubes compared to no-stretch (0%) controls (Figure 2a-d and 2e-h). Of note, for both EDL- and SOL-derived control myotubes only stretch bouts over 3%, showed a significant increase in $[Ca^{2+}]i$. Reduction of *Piezo1* severely suppressed in $[Ca^{2+}]i$ in response to stretch compared to control cells (siRNA controls) (Figures 2a,c and 2b,d). Indeed, the progressive increase in $[Ca^{2+}]i$ was completely abolished in EDL-derived myotubes (Figure 2c) with neither a 6%, nor a 9% stretch eliciting a significant increase in $[Ca^{2+}]i$ (Figure 2c). Similarly, reduction of *Piezo1* in SOL-derived myotubes (Figure 2d), showed a significant decrease in $[Ca^{2+}]i$ at all stretch bouts (Figure 2e), with only *Piezo1*-knockdown myotubes showing increased $[Ca^{2+}]i$ at the 9% stretch condition compared to 3% stretch. Thus, *Piezo1* is essential for Ca^{2+} influx during stretch.

Yoda1-mediated activation of Piezo1 was able to overcome the mechanical threshold imposed in control cohorts. Indeed, at bouts of 3% stretch, EDL- and SOL-derived myotubes treated with Yoda1 (Figure 2e,g and 2f,h) showed a significantly higher $[Ca^{2+}]i$, compared to untreated 3% stretch counterparts. This increase in $[Ca^{2+}]i$ persisted at higher stretch bouts, with both EDL- and SOL-derived myotubes exhibiting higher $[Ca^{2+}]i$ at 6% and 9% stretch bouts compared to untreated stretched counterparts (Figure 2g and h). In summary, Piezo1 expression and activity are crucial for Ca^{2+} regulation in muscle function.

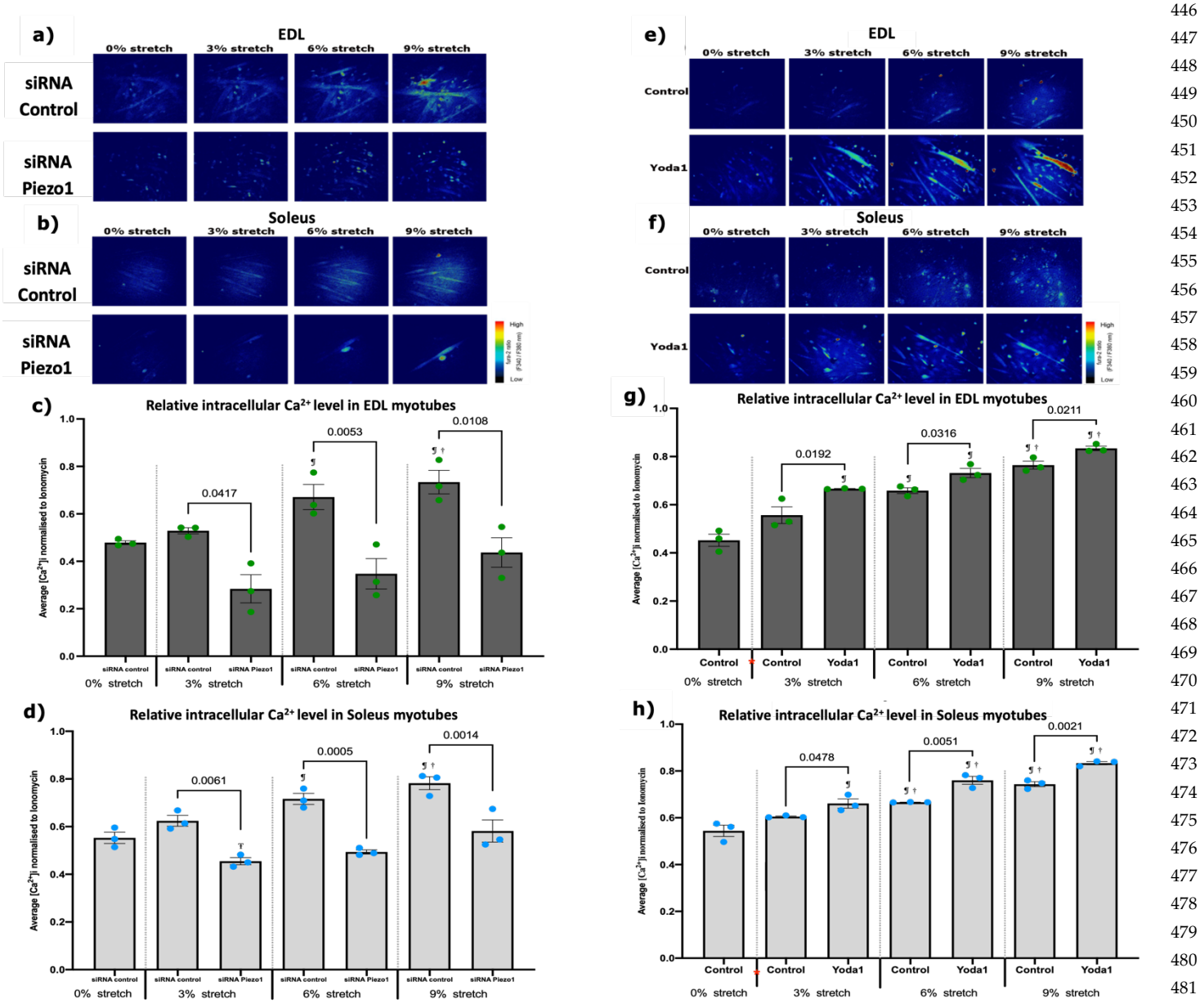

Figure 2. Modulation of Piezo1 alters stretch-mediated increase of intracellular Ca^{2+} in myotubes. (**a**) and (**b**) Representative images of intracellular Ca^{2+} imaging in EDL and SOL-derived myotubes. Myoblasts were transfected with 10 nM of either control-siRNA (top panels) or *Piezo1*-siRNA (bottom panels). After overnight incubation, cells were incubated for a further 72 hours in differentiation medium. Fura 2-AM was administered to myotubes followed by a 30-min incubation time. Stretch was then applied at 3% (0.3 mm), 6% (0.6 mm) and 9% (0.9 mm) for 1 min followed by a 1-min resting period in between. Ionomycin at 5 μM was then applied. Side vertical bar shows Fura 2-AM ratio emittance from low to high. (**c**) and (**d**) Average changes in the intracellular Ca^{2+} level ($[Ca^{2+}]i$) calculated by difference between base and peak pixel value normalised to ionomycin. (**e**) and (**f**) Representative images of Ca^{2+} imaging in EDL and SOL-derived myotubes. Fura 2-AM was administered to myotubes followed by a 30-min incubation time. Stretch was then applied at 3% (0.3 mm), 6% (0.6 mm) and 9% (0.9 mm) for 1 min followed by a 1-min resting period in between. During the initial 0% stretch timepoint, Yoda1 cohorts were administered with 30 μM of the agonist (red *) before being subjected to stretch. Ionomycin at 5 μM was then applied. Side vertical bar shows Fura 2-AM ratio emittance from low to high. (**g**) and (**h**) Average changes in the intracellular Ca^{2+} level ($[Ca^{2+}]i$,), difference between base and peak pixel value normalised to ionomycin. Data is mean ± SEM from three experiments (n = 3 mice). p values are annotated above graphs showing significance compared to control at each stretch condition. ¶: Significant difference at $p < 0.05$ compared to 0% stretch counterparts. †: Significant difference at $p < 0.05$ compared to 3% stretch counterparts. Ŧ: Significant difference at $p < 0.05$ compared to 9% stretch in *Piezo1*-siRNA conditions using one-way ANOVA followed by the Tukey-Kramer post-hoc.

3.3 Piezo1 is dispensable for myoblast proliferation and early commitment to differentiation

Piezo1 expression peaks at later myogenic steps, where it regulates calcium influx during contraction. However, whether Piezo1 participates in earlier phases of myogenesis is unclear. Thus, we set out to evaluate the effects of manipulating *Piezo1* on proliferation and onset of myogenic program. Knockdown of *Piezo1* had no overt effect on the proliferation rate of both EDL- and SOL-derived myoblasts (Supplementary Figure 1c-f), thus *Piezo1* is dispensable for muscle cell proliferation. Next, we investigated whether reduction of *Piezo1* could alter the entrance into differentiation stage by analysing the accumulation of the transcription factor Myogenin. Neither EDL-derived or SOL-derived myoblasts showed a significant difference in the relative proportion of Myogenin-positive cells between *Piezo1*-knockdown and control-siRNA treated conditions (Figure 3a-d), suggesting that *Piezo1* does not participate in the onset of myoblast differentiation. *Piezo1* seemed to exert most of its expression during differentiation, thus in order to address potential compensatory effect of *Piezo2* in response to *Piezo1* knockdown, we measured *Piezo2*`s expression in EDL- and SOL-derived myotubes (Supplementary Figure 1g and 1h). We again confirmed the reliability in our method of siRNA-mediated knockdown by showing significant reduction of *Piezo1* expression in both EDL- and SOL-derived myotubes (Supplementary Figure 1i and 1j). Importantly, RT-qPCR analysis revealed that *Piezo1* knockdown does not alter *Piezo2* expression in EDL- and SOL-derived myotubes (Supplementary Figure 1g and 1h) indicating that *Piezo2* does not compensate for *Piezo1* suppression. Moreover, *Piezo2* expression was extremely low in both EDL and SOL samples, confirming previously published data [5, 21].

Myoblast fusion requires extensive membrane remodelling together with mechanical stress; thus, we next evaluated the effect of *Piezo1* suppression on myotube formation and maturation. Knockdown of *Piezo1* led to a dramatic reduction in myoblast fusion and subsequent hinderance in the formation of both EDL- and SOL-derived myotubes (Figure 3e-3h). In line with reduced myoblast fusion, EDL- and SOL-derived myoblasts (Figure 3i-l) showed reduced expression of the fusogene *Myomaker* [23-28] (Figure 3i and 3k) suggesting alteration of fusion machinery at the molecular level. Expression of *Myomixer* showed a trend to decrease (Figure 3j and 3l). Moreover, knockdown of *Piezo1* in early formed myotubes confirmed a significant reduction in the fusion index, compared to control-siRNA conditions (Figure 3m-p). In summary, dysregulation of *Piezo1* expression reduces the ability of cells to fuse into new or existing myotubes.

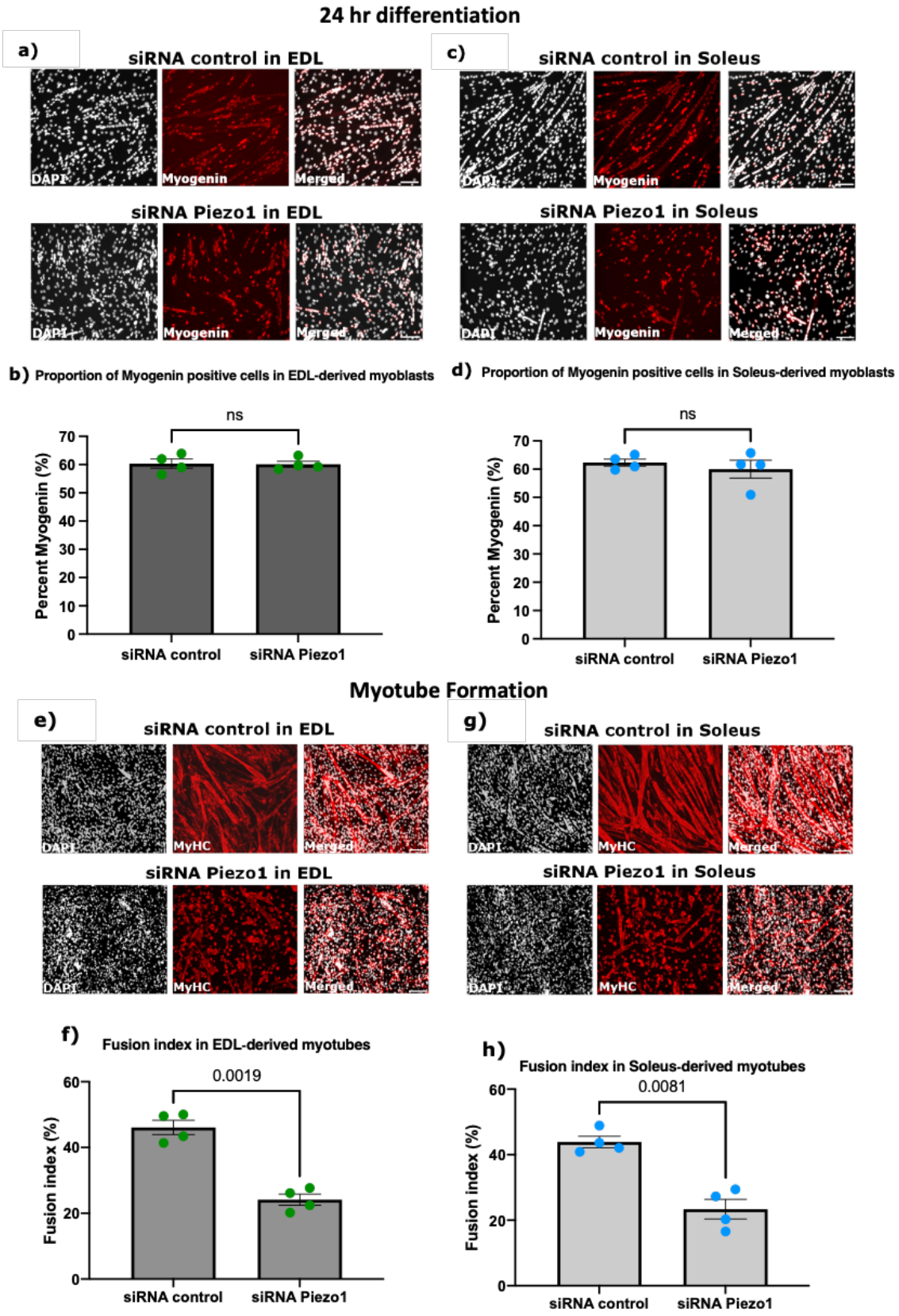

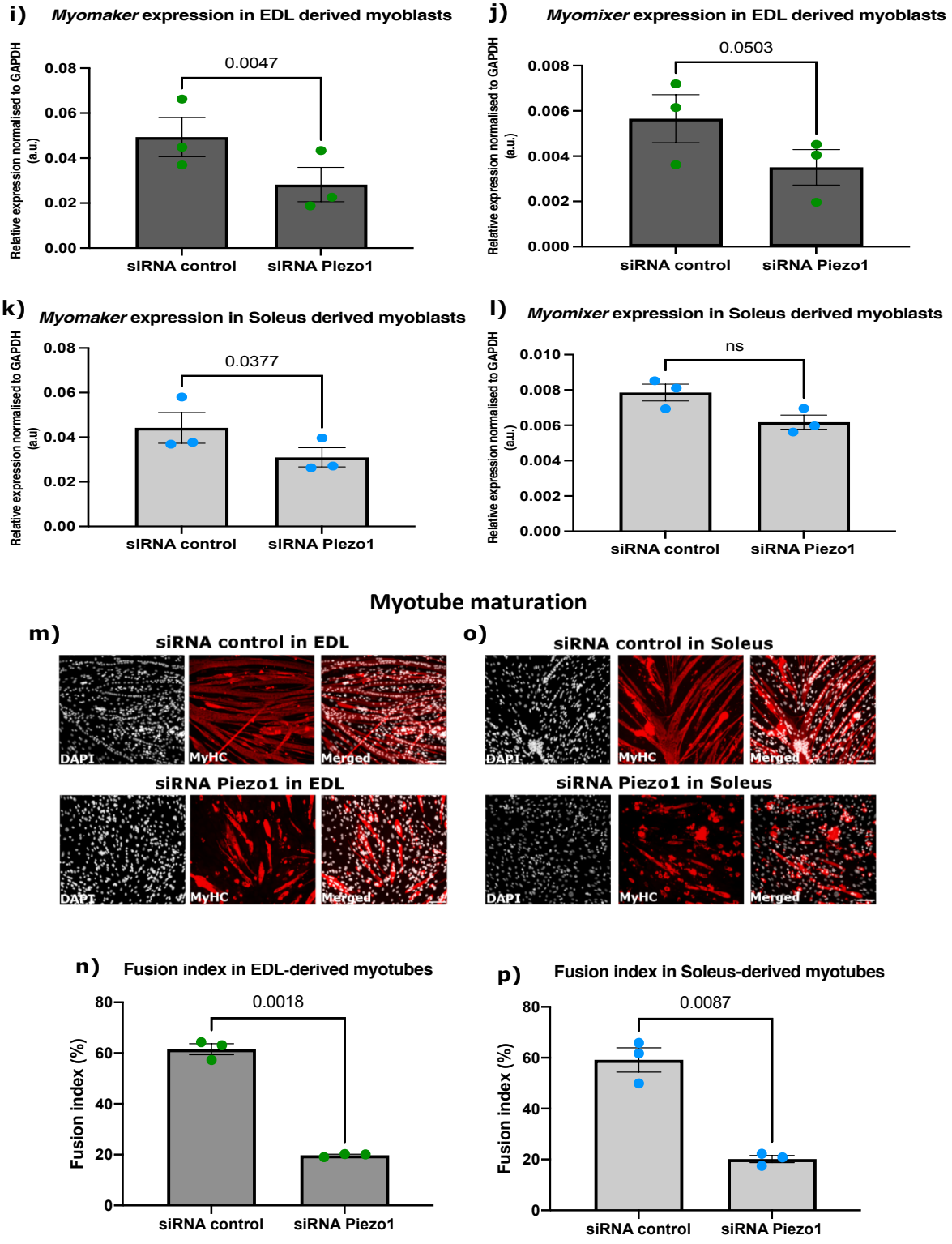

Figure 3. ***Piezo1*** **knockdown reduces myoblast fusion and expression of fusogens.** (**a**) and (**c**) Representative images of EDL and SOL-derived myoblasts transfected with 10nM of control-siRNA (siRNA control) or *Piezo1*-siRNA. Following overnight incubation, cells were incubated for a further 24 hours in differentiation medium, immunolabelled for Myogenin (red panels) and counterstained with DAPI (black and white panels). Scale bar is 100 μm. (**b**) and (**d**) Percentage proportion of Myogenin-positive cells relative to total nuclei. (n = 4 mice). (**e**) and (**g**) Representative images of myotubes from EDL and SOL, transfected with 10nM of control-siRNA or *Piezo1*-siRNA. Following overnight incubation, cells were incubated for a further 72 hours. Cells were immunolabelled for Myosin heavy chain (MyHC) (red panels) and counterstained with DAPI (black and white panels). (**f**) and (**h**) The fusion index was calculated by counting the total number of nuclei within each myotube and representing this as a percentage relative to the total number nuclei in the image taken (n = 4 mice). (**i**

- l) Relative fold changes in expression of EDL-derived myoblasts (**i** and **j**) and SOL-derived myoblasts (**k** and **l**). Cells were transfected with 10 nM of either control-siRNA (siRNA control) or *Piezo1*-siRNA (siRNA *Piezo1*). After overnight incubation, cells were incubated for a further 24 hours. The expression of the fusogenic protein genes *Myomaker* and *Myomixer* were then analysed. Values were normalised to Gapdh. (n = 3 mice). (**m**) and (**o**) Representative images of EDL and SOL-derived myotubes. Early forming myotubes were transfected with 10nM of control-siRNA (siRNA control) or *Piezo1*-siRNA (siRNA-*Piezo1*). Following overnight incubation, cells were incubated for a further 48 hours, immunolabelled for Myosin heavy chain (MyHC) (red panels) and counterstained with DAPI (black and white panels). Scale bar is 100 μm. (**n**) and (**p**) Bar graphs display the fusion index (n = 3 mice). Data is mean ± SEM. p values are annotated above graphs showing significance (or ns, not significant) compared to siRNA control conditions using a 2-tailed paired student t-test.

3.3 Piezo1 activity is finely regulated during myoblast fusion

Knockdown of *Piezo1* reduces myoblast fusion and alters Ca^{2+} influx. Thus, we next assessed the dose-dependent effect of Piezo1 activation. Early forming myotubes were subjected to varying concentrations of Yoda1 over a period of time. After each allocated timepoint, the agonist containing medium was removed and replenished with fresh differentiation medium and incubated for a further 2 days (Figure 4).

Strikingly, a 1-minute treatment of Yoda1 enhanced significantly cell fusion both in EDL- and SOL-derived myotubes at 30 μM and 100 μM of Yoda1 (Figure 4a-d). However, a 30 min treatment with the highest dose (100 μM) of Yoda1 had the opposite effect, reducing fusion index (Supplementary Figure 2), suggesting that Piezo1 activity must be finely tuned to achieve efficient fusion and myotube maturation. Indeed, both EDL- and SOL-derived myotubes incubated at 100 μM beyond the 1 min timepoint, showed a significant decrease in fusion, compared to vehicle-treated controls (Supplementary Figure 2). After 1 h of incubation timepoint, EDL-derived myotubes exhibited increased fusion efficiency at 5 μM, 10μM and 30 μM of Yoda1 treatment, compared to DMSO controls (Figure 4b). Similarly, SOL-derived myotubes incubated with Yoda1 for 1 hour showed an increase in fusion at 5 μM, 10 μM and 30 μM, compared to DMSO controls (Figure 4c and Supplementary Figure 2). Continued Piezo1 activation (4 h) showed a significant decrease in fusion of EDL-derived myotubes at a Yoda1 concentration of 30 μM compared to DMSO control (Supplementary Figure 2a and 2c).

At molecular level, *Piezo1* expression was increased in both EDL- and SOL-derived myotubes post Yoda1 administration (Supplementary Figure 6a and 6b). *Myomaker* expression also paralleled *Piezo1* upregulation in both EDL- and SOL-derived myotubes (30 μM 30 min incubation and 10μM 1 h incubation). Interestingly *Myomixer*, although showed a trending increase in expression, did not reach statistical significance. Taken together, our data show that fine regulation of Piezo1 activity is a key step during differentiation dynamics.

We noticed that induced activation of Piezo1 appeared to affect myotube size, although increasing myoblast fusion. In order to address this, we compared the myotube width of these samples to DMSO controls (Figure 4e-h). Interestingly, both EDL- (Figure 4e and 4f) and SOL-derived myotubes (Figure 4g and 4h) showed reduced myotube width compared to controls when treated with Yoda1. Both EDL- and SOL-derived myotubes, showed that Yoda1 treated cells, on average, have a greater proportion of smaller myotubes (Figure 4i-j) compared to controls which have a higher distribution of lager myotubes. A similar pattern was observed in the rest of the Yoda1 treated cohorts that displayed increased fusion (Supplementary Figure 3). Taken together, over activation of Piezo1 unbalances myoblast fusion and myotube size.

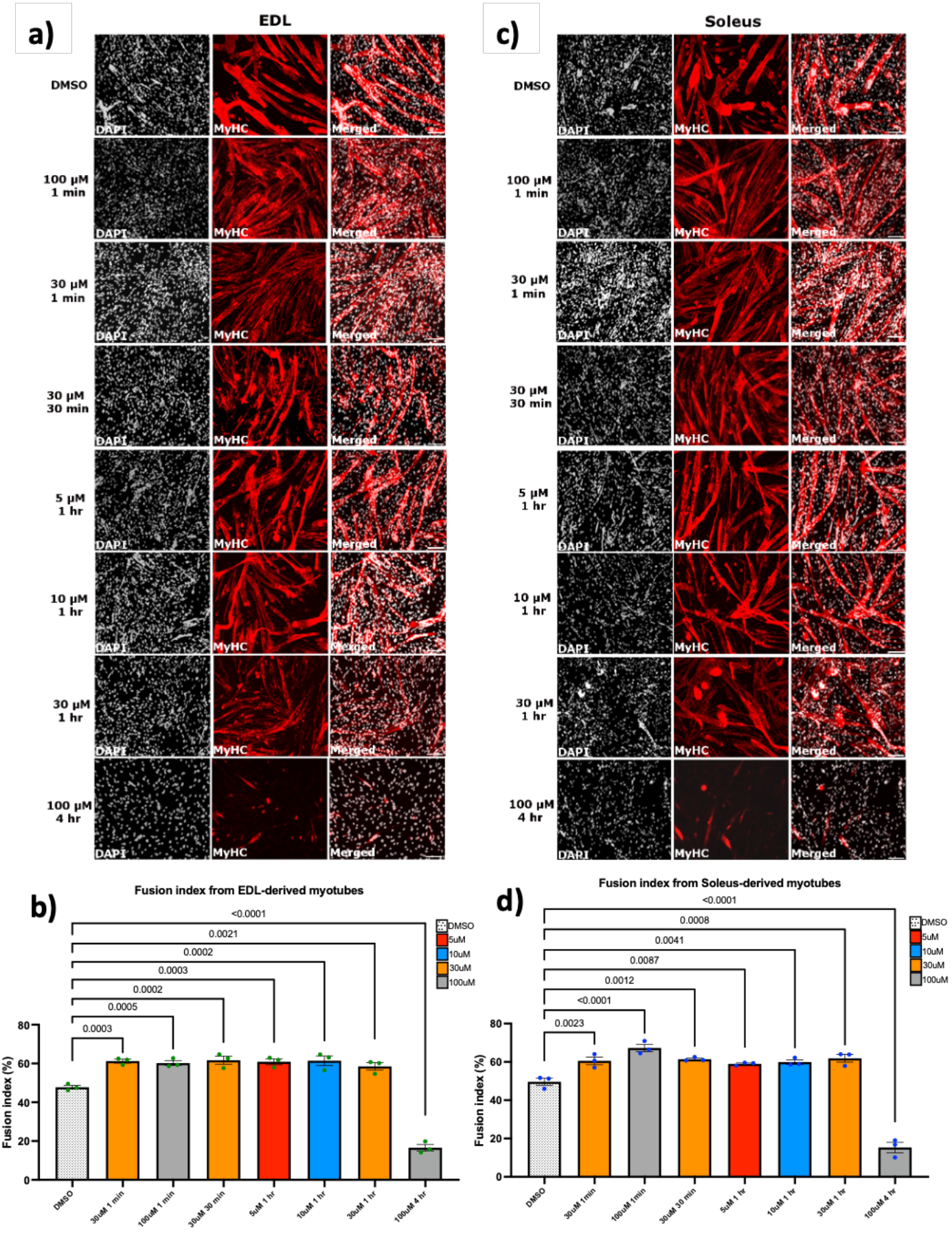

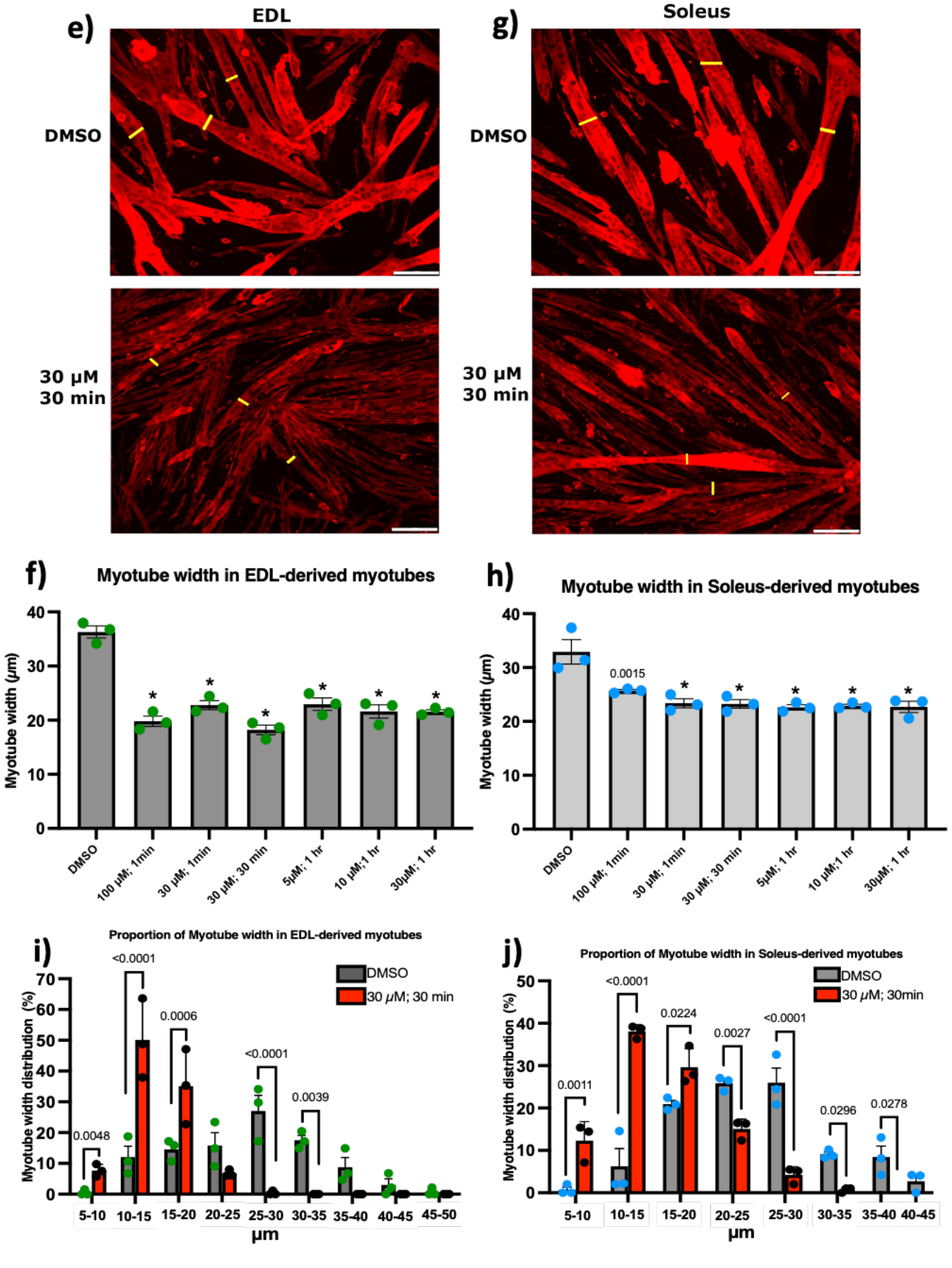

Figure 4. Piezo1 activation increases myoblast **fusion at the expense of myotube syncytial maturation.** (**a**) and (**c**) Representative images of cohorts at relevant timepoints and concentrations, immunostained for Myosin heavy (MyHC) (red panels) and counterstained with DAPI (black and white panels). Micrographs taken at x20 magnification. Scale bar is 100 μm. (**b**) and (**d**) Bar graphs displaying fusion index in EDL- and SOL-derived myotubes at the relevant time point and concentration variables. Yoda1 values are compared to DMSO controls at 1 min. Please refer to Supplementary Figure 2 for cross comparison of all concentrations against their respective controls at each timepoint. (**e**) and (**g**) Representative images of EDL- and SOL-derived myotubes immunolabelled for MyHC. We measured the width of the myotubes to quantify potential differences between Piezo1-activated cohorts (lower panels) and DMSO controls (upper panels). This was achieved by taking three independent points within a field of view (yellow bars) and measuring the distance from one side of the myotube to the other. Example pictures from DMSO controls and 30 μM of Yoda1 incubated for 30 min are displayed. Scale bar is 100 μm. (**f**) and (**h**) Average myotube width in DMSO and Piezo1 activated samples. (**i**) and (**j**) Proportion of myotube width in EDL- and SOL-derived myotubes. Myotube width was divided into incremental bins of 5 μm and represented as percentages relative to the total number of myotubes counted. Values are mean ± SEM. p values are annotated above graphs showing significance compared to DMSO controls using one-way ANOVA tests followed by the Tukey-Kramer post-hoc. n = 3 mice. For (f) and (h) asterisks (*) denote significance at $p < 0.0001$ compared to DMSO controls conditions. Please note that only cohorts which showed increased myoblast fusion in both EDL- and SOL-derived myotubes from Figure 4a-d are displayed.

3.4 Deregulation of Piezo1 alters cytoskeletal remodelling during differentiation

Along with myoblast fusion, myogenic differentiation requires extensive cellular remodelling, and previous research places Piezo1 regulation as a key player in cytoskeletal homeostasis [22, 23]. To understand whether Piezo1 contributes to regulate cytoskeletal structures, including f-actin, we examined f-actin accumulation as a proxy to evaluate the extent of cytoskeletal reorganisation during myogenic differentiation in EDL- and SOL-derived myotubes. *Piezo1*-knockdown showed a significant decrease in the accumulation of f-actin compared to control-siRNA (Supplementary Figure 4a-d), suggesting that reduction of *Piezo1* alters cytoskeletal dynamics. In contrast, f-actin accumulation was unaffected by Piezo1 over-activation (Supplementary Figure 4e-h), suggesting that Piezo1 may not directly contribute to f-actin remodelling. In line with alteration in myoblast fusion, excessive chemical activation of Piezo1 showed a significant decrease in f-actin in EDL (100 μM; 4-hour incubation) and SOL (100 μM; 30-min, 1- and 4-hour incubation) -derived myotubes (Supplementary Figure 4f and 4h). These findings suggest that deregulation of *Piezo1* expression and/or its activation status may impinge, likely indirectly, on cytoskeletal organisation during muscle differentiation.

4. Discussion

Our study reveals that the mechanosensitive ion channel Piezo1 is finely tuned during the myoblast fusion and formation of myotubes through four main findings. 1) *Piezo1* expression increases during myoblast differentiation in a muscle-type independent fashion. 2) *Piezo1* is essential for proper Calcium influx during muscle contraction. 3) Modulation of *Piezo1* expression alters both myoblast fusion and expression of the fusogens *Myomaker* and *Myomixer*. 3) Over-activation of Piezo1 disbalances myoblast fusion and myotube width.

Piezo1 in myogenesis

The current study investigated the effects of Piezo1 regulation throughout the myogenic program. *Piezo1* is expressed at a higher proportion in terminally differentiated myotubes, compared to proliferating myoblasts. Moreover, we found that, differentiating myocytes derived from the mainly slow-type muscle SOL displayed higher expression of *Piezo1* compared to the fast EDL muscle. Understanding the potential differences in muscle/fibre types and *Piezo1* regulation is an intriguing area for future research and could reflect differences in the dynamics of myogenic progression. We also confirmed that the expression of *Piezo2* is not altered by the down-regulation of *Piezo1*. This is perhaps not surprising given the fact that *Piezo2* is not as abundant in skeletal muscle compared to

Piezo1 [5, 21]. Nevertheless, it was important to see any potential compensatory effects *Piezo2* may impose. Specific downregulation of *Piezo1* by siRNA-mediated transfection showed no significant change in the proliferation rate of either EDL- or SOL-derived myoblasts. However, our data do not exclude the possibility that Piezo1 is not involved in earlier myogenic events, perhaps in balancing quiescence and activation of SCs. In proliferating myoblasts, reduction of Piezo1 function does not alter onset of myoblast differentiation, evaluated by the proportion of Myogenin-positive cells. However, that is not to say that perhaps Piezo1 does not alter other events important to myoblasts such as cell motility, which the current study did not include. In our current study, where a significant phenotype was observed was in terminally differentiated myotubes. Indeed, our data found that knockdown of *Piezo1* significantly reduced fusion of myocytes and prevented myotube formation and maturation. In contrast, activation of this Ca^{2+} permeable channel resulted in enhanced myoblast fusion.

Piezo1 activation and Ca^{2+} influx

We show that selective downregulation of *Piezo1* dramatically suppressed $[Ca^{2+}]i$, which most likely translates in the depression of the influx of Ca^{2+} into cultured myotubes exposed to stretch. In contrast, activation of Piezo1 significantly increased $[Ca^{2+}]i$, which means the enhancement of Ca^{2+} influx. Our results propose that Piezo1 is a novel intracellular Ca^{2+} regulatory protein in skeletal muscle function. Ca^{2+} plays a crucial role in skeletal muscle function, maintenance and plasticity. All myofibres use Ca^{2+} as their main regulatory and signalling molecule [18-20]. Therefore, the contractile functionalities of myofibres are dependent on the highly regulated expression of proteins involved in Ca^{2+} handling and signalling. Our study showed that Piezo1 mediated regulation of Ca^{2+} influx is a key driving factor in the respective decrease and increase in myoblast fusion in response to Piezo1 inhibition and activation. To the best of our knowledge this is the first time this has been demonstrated.

The silicon bio-chamber experiments revealed that at relatively low stretch conditions of 3% (0.3 mm) neither EDL- nor SOL-derived myotubes elicited a significant increase in Ca^{2+} influx. However, at higher stretch distances (6% and 9% stretch) this mechanical barrier was crossed as demonstrated by the net increase in $[Ca^{2+}]i$, compared to 0% stretch counterparts. In a similar set of experiments (albeit using urothelial cells), Miyamoto et al. also showed a distance dependent increase of Ca^{2+} influx. Interestingly this response was blunted in *Piezo1*-siRNA-treated conditions [21]. The researchers also showed that a high enough $[Ca^{2+}]i$ must be attained in order to elicit a response, in their case ATP efflux. Our data support the presence of a stretch-dependent increase in Ca^{2+} influx. Remarkably we found that activation of Piezo1 resulted in increased $[Ca^{2+}]i$ at 3% stretch conditions, suggesting that the activation threshold of Piezo1 was lowered. Furthermore, the data showed that reduction of *Piezo1* expression significantly blunted any significant increase of $[Ca^{2+}]i$ in response to stretch. These results, for the first time show the need for Piezo1 to respond to stretch and permeate Ca^{2+} into myotubes. The findings also propose the presence of a physical threshold that must be attained before Piezo1 mediated Ca^{2+} influx is significantly increased. Moreover, like Miyamoto et al [24], we find that a stretch-dependent increase in Ca^{2+} influx is suppressed when *Piezo1* expression is decreased. Conversely, we see an increase of $[Ca^{2+}]i$ when Piezo1 is activated. Whether this leads to altered cellular/myotube viability in the form of ATP release remains a subject for future research.

Piezo1 and muscular dystrophies

Piezo1 activation showed a significant increase in the fusion index of both EDL- and SOL-derived myotubes. Although this phenotype could be viewed as beneficial in terms of muscular dystrophy prevention, we must be aware of the potential dangers of an overactive Piezo1 channel. In fact, we showed that even a 30 min incubation of myotubes with a high agonist concentration (100 μM of Yoda1 treatment) led to decreased fusion in both

EDL- and SOL-derived myotubes (Supplementary Figure 2). This adverse phenotype is most likely the result of a dangerously high Ca^{2+} influx. Indeed, Since the early 1990's it has been postulated that defective mechanotransductors, also referred to stretch activated channels (SACs), contribute to the high influx of Ca^{2+}, and hence maintain higher Ca^{2+} resting levels in Duchenne's muscular dystrophy (DMD) [14, 25]. However, the identity of this channel(s) in DMD is yet to be identified. The current data makes the hypothesis that DMD stricken muscle may have malfunctioning Piezo1 channels which permeate Ca^{2+} at hazardously high levels. It is possible that the reduced fusion we observed from an over-active Piezo1 channel (Figure 4 and Supplementary Figure 2) stems from one of the many defects caused by over-accumulation of Ca^{2+}. It is imperative that future experiments characterise the expression of Piezo1 not only in DMD but other muscular dystrophies. This work is currently underway.

Piezo1 and the myoblast fusion machinery

Piezo1 downregulation significantly reduced myoblast fusion during myotube formation and myotube maturation. To the best of our knowledge there is only one other paper published that examined *Piezo1* in skeletal muscle by Tsuchiya et al. [26]. Interestingly, the findings from this group showed that *Piezo1* inhibition resulted in a sheet-like syncytium of MyHC coupled with increased fusion. Although these findings show contrasting results to the ones presented in this study, we must take into consideration potential factors which may explain why this may be the case. One such factor is the method of *Piezo1* inhibition used by Tsuchiya et al, [26]. They carried out many of their experiments using knockout lines of *Piezo1* through the gene editing tool CRISPR/Cas9. The fact that these cell lines did not express *Piezo1* to begin with (unlike the cells we used) may yield completely different phenotypes, compared to the transient inhibition achieved by siRNA mediated transfection. Therefore, complete lack of *Piezo1* expression may favour the activation of a secondary, yet unknown, alternative *Piezo1*-affected pathway(s) to fusion as observed for other factors involved in fusion, such as Myogenin [27]. Regarding the *Piezo1* siRNA transfection experiments, although more than 60% reduction in gene expression is ideal; we nevertheless found that our level of *Piezo1* knockdown produced very interesting effects on myogenic regulation. Moreover, Miyamoto et al, [21] also obtained slightly below or just about 60% *Piezo1* reduction, yet reported intriguing *Piezo1*-associated events in urothelial cells. Perhaps Tsuchiya et al, obtained even greater knockdown of *Piezo1* in their siRNA-mediated analyses [26], further suggesting that the timing and level of *Piezo1* expression may yield varying phenotypes. There was also the likelihood that siRNA used in this study may potentially have off-target effects on other genes which could influence myotube formation by employing other mechanistic pathways. However, this likelihood is reduced by the fact that we have now tested five different *Piezo1*-specific siRNAs (including the one used by Tsuchiya et al. from the company Sigma) and all show reduced fusion (Supplementary Figure 5). Nevertheless, this study welcomes falsifiability. In fact, the siRNA used from Sigma, despite showing reduced fusion compared to controls, did show significantly greater fusion index compared to some of the siRNAs used from the company Qiagen. Furthermore, the knockdown efficiency measured by RT-qPCR showed that the Sigma-derived *Piezo1* siRNA was on average even more efficient compared to the main siRNA from Qiagen used in this study (Supplementary Figure 5f and 5g). Thus, our report highlights the potential phenotypic differences from fine tuning *Piezo1* downregulation levels. At the very least this report highlights the potential danger in using siRNAs solely from one provider and demands further high-quality testing from these companies to reduce potential off-target effects.

Additional support for the involvement of Piezo1 in myoblast fusion comes from our results which showed that its downregulation significantly reduced the expression of *Myomaker* - a muscle specific protein that localises to the plasma membrane and is crucial for vertebrate myoblast fusion [28-31]. Conversely Yoda1 specific activation of Piezo1 showed increased *Myomaker* expression (Supplementary Figure 6) indicating an interplay

between *Piezo1* and *Myomaker*. *Myomixer* on the other hand did not show significant changes in expression post downregulation nor activation of Piezo1. This potential decoupling of these fusogenic proteins is line with previous findings from Leikina et al [32]. Future studies should uncover whether the respective decrease and increase in *Myomaker* expression is a direct response from the downregulation/activation of Piezo1 or an indirect event paralleling altered fusion pathway.

5. Conclusions

The data presented in this study showed that the Piezo1 channel is present in SC-derived myoblasts and myotubes but expressed at a higher proportion in the latter. Downregulation of *Piezo1* significantly lowered the fusion capacity during myotube formation and maturation. In contrast, Piezo1 activation increased fusion. Future research examining changes in myotube function (integrity, Ca^{2+} influx, cytoskeletal organisation and fusion) that are directly the result of mechanical stress should consider analysis of Piezo1. In the context of therapeutic strategies against muscular dystrophies such as DMD, not only must we unravel the spatiotemporal regulation of *Piezo1* expression, but we must be aware of this channel's ability to alter its Ca^{2+} influx threshold by adapting or inactivating its gating capacity in response to repetitive stimuli. Pharmaceutically, small activating molecules such as Yoda1 (and others like it) may prove beneficial. However careful attention must be given to the half-life and pharmacokinetics of these agonists in vivo before even considering them as viable drugs for human consumption. Piezo1's importance in skeletal muscle maintenance and function will undoubtedly grow as new research aims to explore the mechanisms and signalling pathways this remarkable mechanosensor employs.

Author Contributions: K.G. designed and organized this study and performed data analysis as well as editing and review of manuscript. H.P.O.Q. wrote the manuscript, performed the experiments and performed data analysis. M.G. contributed to writing and editing manuscript and data analysis. S.Y. performed experiments. K.N. helped with experiments. T.Y. helped with experiments. D.R. helped with experiments. A.H. helped with experiments. O.H. helped with experiments. J.B. helped with experiments. A.A. helped with reviewing and editing of manuscript. Y.S. helped with reviewing and editing manuscript. M.T. provided experimental support and equipment and reviewed and edited manuscript. P.S.Z. provided advise, discussion support and reviewed and edited manuscript.

Funding: This work was supported by KAKENHI (JP17K01762, K.G.; JP18H03160, K.G.; JP19K22825, K.G.; 19KK0254. K.G.) from the Japan Society for the Promotion of Science, the Science Research Promotion Fund from the Promotion and Mutual Aid Corporation for Private Schools of Japan, and Graduate School of Health Sciences, Toyohashi SOZO University (K.G.).

Institutional Review Board Statement: All experimental procedures were carried out in accordance with the Guide for the Care and Use of Laboratory Animals as adopted and promulgated by the National Institutes of Health (Bethesda, MD, USA) and were approved by the Animal Use Committee of Toyohashi SOZO University A2018006, A2019006).

Data Availability Statement: All data is available upon request.

Acknowledgments: The authors thank Ms. Yumiko Asakura from the Department of Physiology, Graduate School of Health Sciences, Toyohashi SOZO University for her assistance.

Conflicts of Interest: The authors declare that there are no conflicts of interest.

References

1. Mauro, A., *Satellite cell of skeletal muscle fibers.* J Biophys Biochem Cytol, 1961. **9**: p. 493-5.
2. Zammit, P.S., et al., *Pax7 and myogenic progression in skeletal muscle satellite cells.* J Cell Sci, 2006. **119**(Pt 9): p. 1824-32.
3. Zammit, P.S., T.A. Partridge, and Z. Yablonka-Reuveni, *The skeletal muscle satellite cell: the stem cell that came in from the cold.* J. Histochem. Cytochem., 2006. **54**: p. 1177-1191.
4. Relaix, F. and P.S. Zammit, *Satellite cells are essential for skeletal muscle regeneration: the cell on the edge returns centre stage.* Development, 2012. **139**(16): p. 2845-56.
5. Coste, B., et al., *Piezo1 and Piezo2 are essential components of distinct mechanically activated cation channels.* Science (New York, N.Y.), 2010. **330**(6000): p. 55-60.
6. Wang, Y., et al., *A lever-like transduction pathway for long-distance chemical- and mechano-gating of the mechanosensitive Piezo1 channel.* Nature communications, 2018. **9**(1): p. 1300-1300.
7. Cinar, E., et al., *Piezo1 regulates mechanotransductive release of ATP from human RBCs.* Proceedings of the National Academy of Sciences of the United States of America, 2015. **112**(38): p. 11783-11788.
8. Ge, J., et al., *Architecture of the mammalian mechanosensitive Piezo1 channel.* Nature, 2015. **527**: p. 64.
9. Sachs, F., *Stretch-activated ion channels: what are they?* Physiology (Bethesda, Md.), 2010. **25**(1): p. 50-56.
10. Saotome, K., et al., *Structure of the mechanically activated ion channel Piezo1.* Nature, 2017. **554**: p. 481.
11. Zhao, Q., et al., *The mechanosensitive Piezo1 channel: a three-bladed propeller-like structure and a lever-like mechanogating mechanism.* Febs j, 2018.
12. Zhao, Q., et al., *Structure and mechanogating mechanism of the Piezo1 channel.* Nature, 2018. **554**: p. 487.
13. Coste, B., et al., *Piezo1 ion channel pore properties are dictated by C-terminal region.* Nature Communications, 2015. **6**(1): p. 7223.
14. Franco-Obregón, A. and J. Lansman, *Calcium entry through stretch-in-activated ion channels in MDX myotubes.* Nature, 1990. **344**: p. 670-3.
15. Mercuri, E., C.G. Bönnemann, and F. Muntoni, *Muscular dystrophies.* Lancet, 2019. **394**(10213): p. 2025-2038.
16. Collins, C.A. and P.S. Zammit, *Isolation and grafting of single muscle fibres.* Methods Mol Biol, 2009. **482**: p. 319-30.
17. Lacroix, J.J., W.M. Botello-Smith, and Y. Luo, *Probing the gating mechanism of the mechanosensitive channel Piezo1 with the small molecule Yoda1.* Nature Communications, 2018. **9**(1): p. 2029.
18. Berchtold, M.W., H. Brinkmeier, and M. Muntener, *Calcium ion in skeletal muscle: its crucial role for muscle function, plasticity, and disease.* Physiol Rev, 2000. **80**(3): p. 1215-65.
19. Gehlert, S., W. Bloch, and F. Suhr, *Ca2+-dependent regulations and signaling in skeletal muscle: from electro-mechanical coupling to adaptation.* International journal of molecular sciences, 2015. **16**(1): p. 1066-1095.
20. Allen, D.G., G.D. Lamb, and H. Westerblad, *Skeletal muscle fatigue: cellular mechanisms.* Physiol Rev, 2008. **88**(1): p. 287-332.
21. Miyamoto, T., et al., *Functional role for Piezo1 in stretch-evoked Ca(2)(+) influx and ATP release in urothelial cell cultures.* J Biol Chem, 2014. **289**(23): p. 16565-75.
22. Nourse, J.L. and M.M. Pathak, *How cells channel their stress: Interplay between Piezo1 and the cytoskeleton.* Semin Cell Dev Biol, 2017. **71**: p. 3-12.
23. McHugh, B.J., et al., *Loss of the integrin-activating transmembrane protein Fam38A (Piezo1) promotes a switch to a reduced integrin-dependent mode of cell migration.* PloS one, 2012. **7**(7): p. e40346-e40346.
24. Miyamoto, T., et al., *Functional Role for Piezo1 in Stretch-evoked Ca2+ Influx and ATP Release in Urothelial Cell Cultures.* The Journal of biological chemistry, 2014. **289**.
25. Franco-Obregon, A., Jr. and J.B. Lansman, *Mechanosensitive ion channels in skeletal muscle from normal and dystrophic mice.* J Physiol, 1994. **481 (Pt 2)**: p. 299-309.

26. Tsuchiya, M., et al., *Cell surface flip-flop of phosphatidylserine is critical for PIEZO1-mediated myotube formation.* Nature Communications, 2018. **9**(1): p. 2049.
27. Ganassi, M., et al., *Myogenin promotes myocyte fusion to balance fibre number and size.* Nature Communications, 2018. **9**(1): p. 4232.
28. Millay, D.P., et al., *Myomaker is a membrane activator of myoblast fusion and muscle formation.* Nature, 2013. **499**(7458): p. 301-5.
29. Ganassi, M. and S. Badodi, *Myogenin promotes myocyte fusion to balance fibre number and size.* 2018. **9**(1): p. 4232.
30. Shi, J., et al., *Knockout of myomaker results in defective myoblast fusion, reduced muscle growth and increased adipocyte infiltration in zebrafish skeletal muscle.* Human Molecular Genetics, 2018. **27**(20): p. 3542-3554.
31. Goh, Q. and D.P. Millay, *Requirement of myomaker-mediated stem cell fusion for skeletal muscle hypertrophy.* 2017. **6**.
32. Leikina, E., et al., *Myomaker and Myomerger Work Independently to Control Distinct Steps of Membrane Remodeling during Myoblast Fusion.* Dev Cell, 2018. **46**(6): p. 767-780.e7.

List of Supplementary Material

Supplementary figure 1. *Piezo1* is expressed in SC-derived myoblasts throughout myoblast differentiation. *Piezo1* downregulation does not alter the expression of *Piezo2*

Supplementary figure 2. Piezo1 activation increases myogenic fusion

Supplementary figure 3. Yoda1-mediated activation of Piezo1 decreases myotube width

Supplementary figure 4. *Piezo1* knockdown reduced f-actin intensity in EDL- and SOL-derived myotubes

Supplementary figure 5. Different *Piezo1* siRNA targets continue to show decrease in myoblast fusion

Supplementary figure 6. *Myomaker* is upregulated in response to Piezo1 activation

Supplementary Figure 1 - *Piezo1* is expressed in SC-derived myoblasts throughout myoblast differentiation. *Piezo1* downregulation does not alter the expression of *Piezo2*

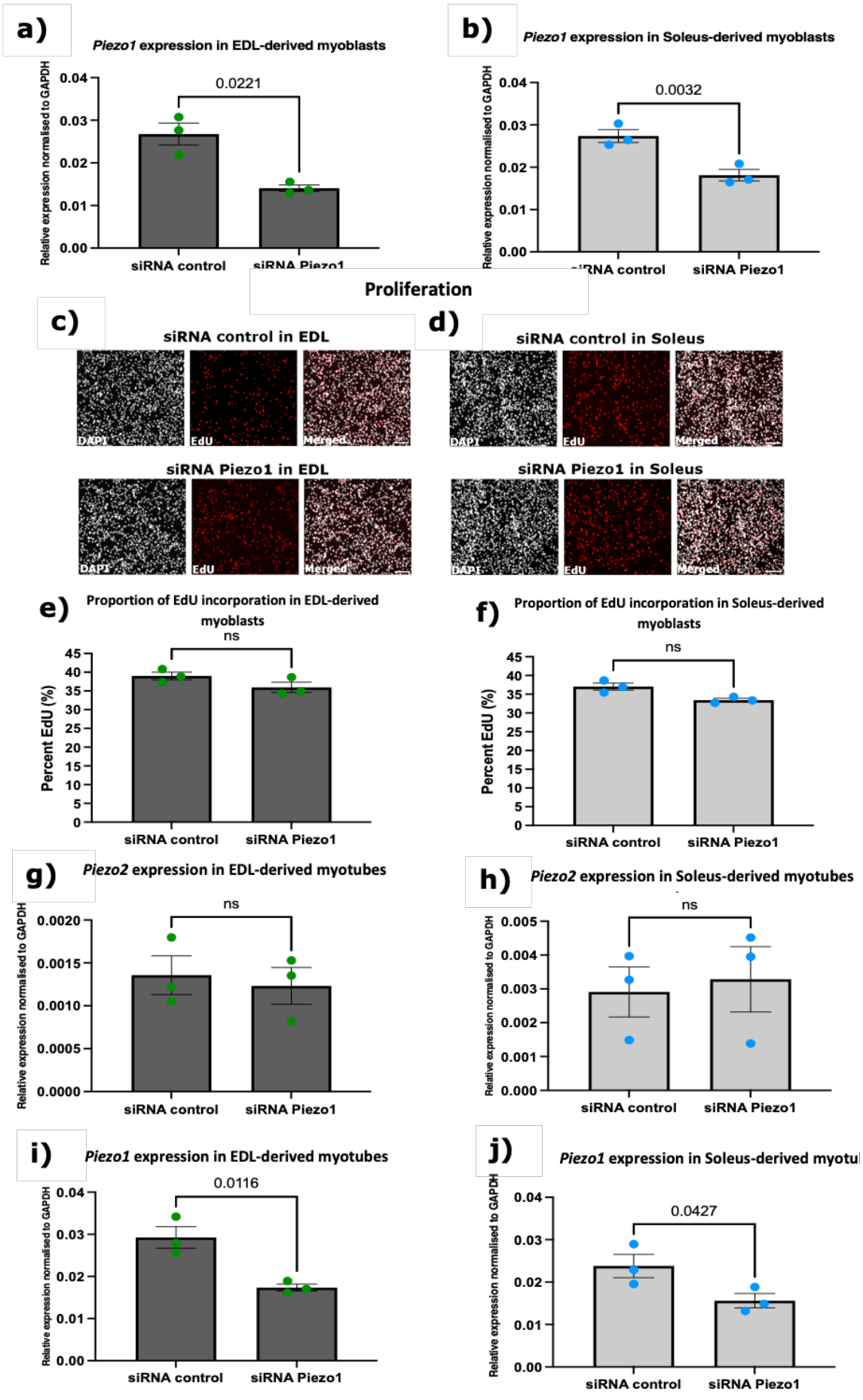

Supplementary figure 1. *Piezo1* is expressed in SC-derived myoblasts throughout myoblast differentiation. *Piezo1* downregulation does not alter the expression of *Piezo2*. (**a**) and (**b**) Relative fold changes in expression of *Piezo1* in murine EDL- (dark grey bars, green dots) and SOL-derived myoblasts (light grey bars, blue dots). myoblasts were transfected with 10 nM of either control-siRNA or targeting siRNA against *Piezo1* (Piezo1-siRNA). After overnight incubation, cells were incubated for a further 24 hours and expression of Piezo1 was measured. (**c**) and (**d**) Representative images of EDL and soleus primary-derived myoblasts, transfected with 10nM of siRNA control or siRNA-Piezo1. Following overnight incubation, the medium was changed with fresh proliferation medium and cells were incubated for a further 24 hours, and then subjected to a 2-hour pulse with EdU (red panels). DAPI counterstained nuclei shown in black and white panels. Scale bar is 100 μm. (**e**) and (**f**) Proportion of EdU-incorporated cells relative to total (DAPI) cell count. (**g-j**) Relative fold changes in expression of *Piezo2* (**g** and **h**) and *Piezo1* (**i** and **j**) in EDL- and soleus-derived **myotubes**. Following an initial differentiation period (24 hours at high confluency), cells were transfected with 10 nM of either control-siRNA (siRNA control) or Piezo1-siRNA. After overnight incubation, cells were incubated for a further 24 hours. Values were normalised to *Gapdh*. Data is presented as mean ± SEM from three experiments (n = 3 mice). p values are annotated above graphs showing significance (or ns, not significant) compared to control conditions using a 2-tailed paired student t-test.

Supplementary Figure 2 - Piezo1 activation increases myogenic fusion

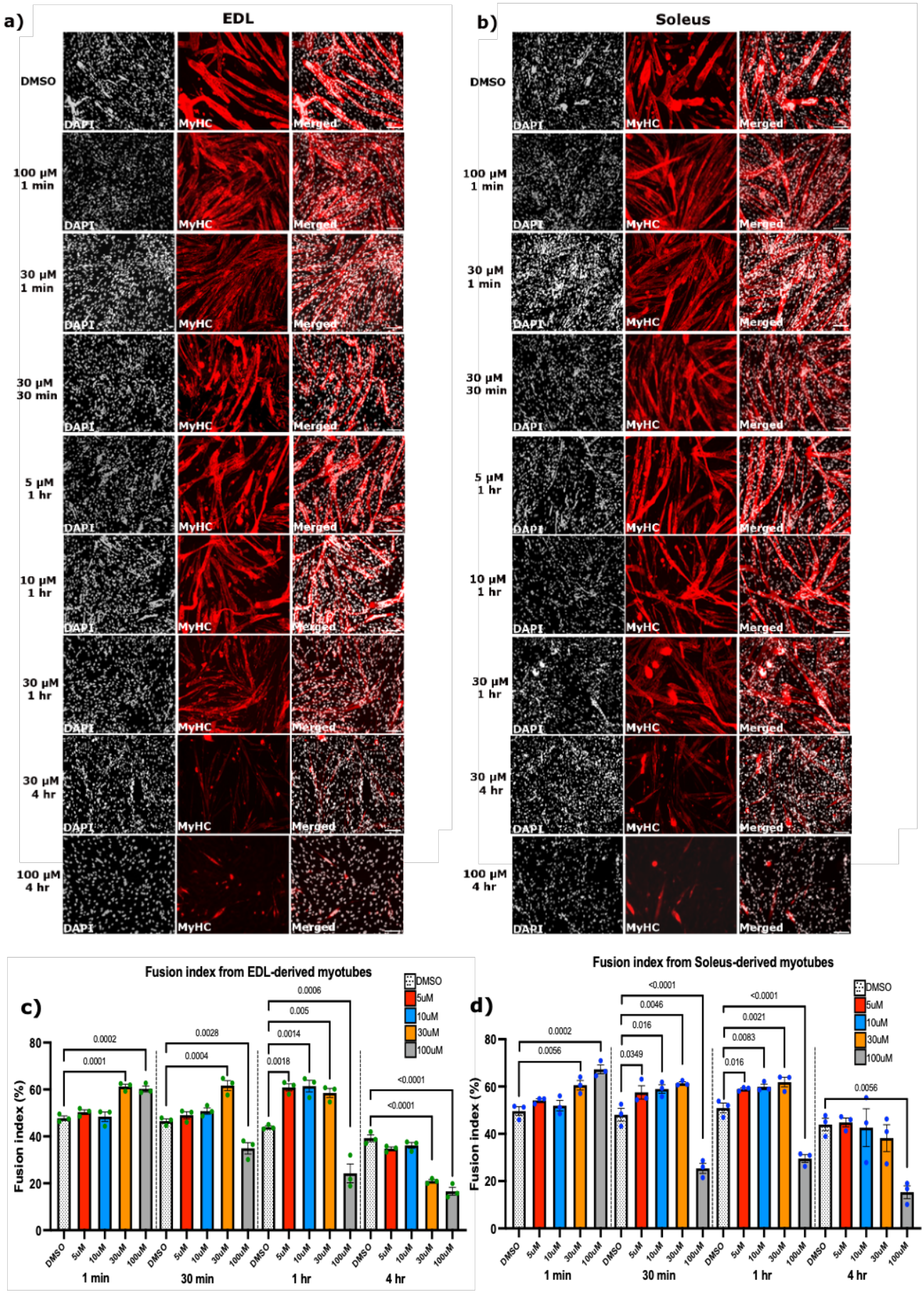

Supplementary Figure 2. Piezo1 activation increases myogenic fusion. Early forming myotubes were administered with either DMSO (control, white dotted bars) or the Piezo1-agonist Yoda1 at the following concentration: 5 μM (red bars), 10 μM (blue bars), 30 μM (orange bars) and 100 μM (grey bars). Myotubes were incubated for 1 min, 30 min, 1 hour and 4 hours. Following the incubation period, the medium was exchanged with fresh reduced medium (without agonist) and myotubes were incubated for a further 2 days. (**a**) and (**b**) Representative images of cohorts at relevant timepoints and concentrations, immunostained for Myosin heavy (MyHC) (red panels) and counterstained with DAPI (black and white panels). Micrographs taken at x20 magnification. Scale bar is 100 μm. Bar graphs display fusion index in (**c**) EDL and (**d**) soleus-derived myotubes from each time point and concentration variables. Values are mean ± SEM. p values are annotated above graphs showing significance compared to DMSO controls using one-way ANOVA tests followed by the Tukey-Kramer post-hoc. n = 3 mice.

Supplementary Figure 3 - Yoda1-mediated activation of Piezo1 decreases myotube width

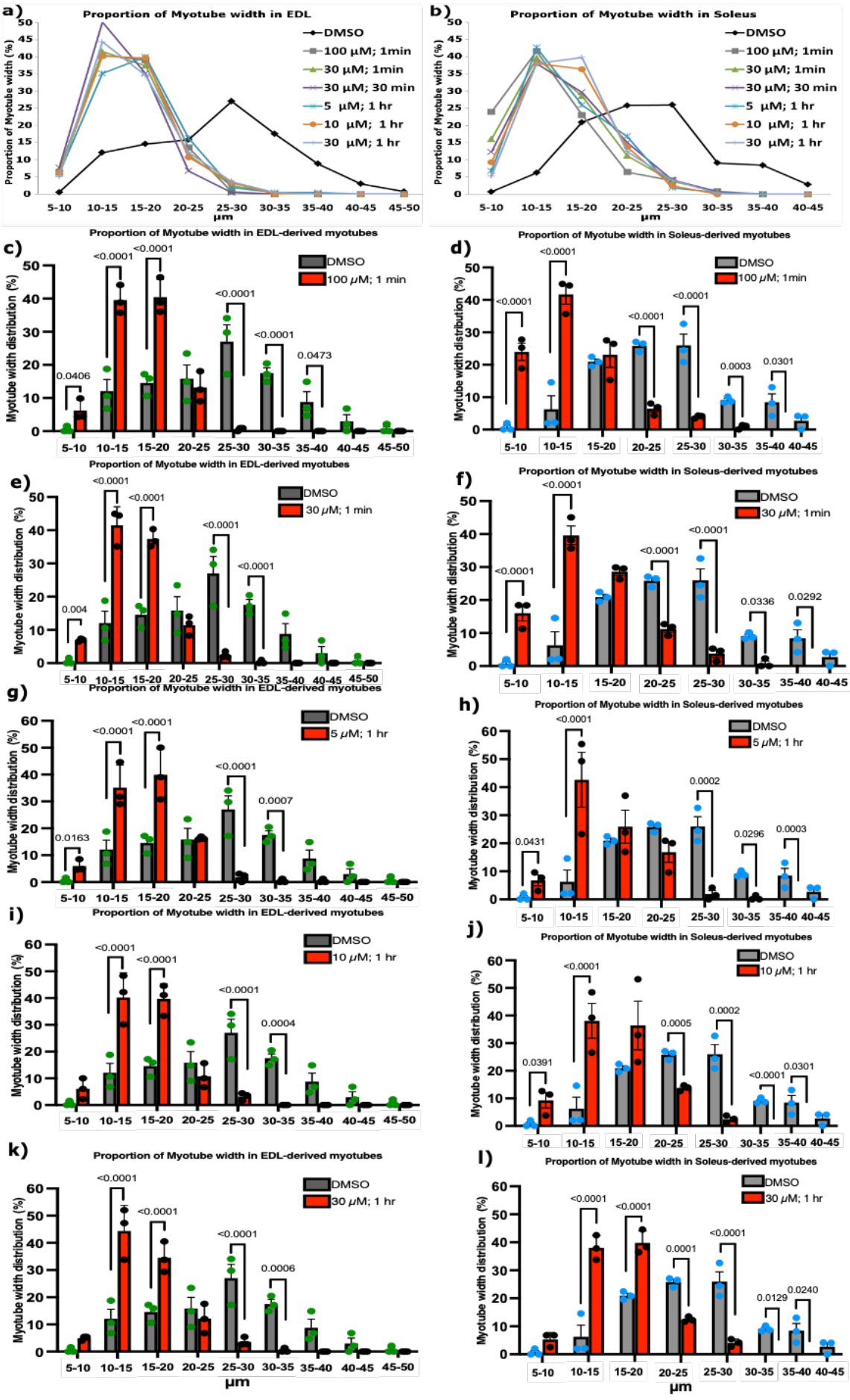

Supplementary Figure 3. Yoda1-mediated activation of Piezo1 decreases myotube width. Myotube width was divided into incremental bins of 5 μm and represented as percentages relative to the total number of myotubes counted. The overall proportion of myotube width distribution in DMSO controls and Yoda1-treated samples is summarised as line graphs in (**a**) EDL and (**b**) soleus-derived myotubes. (**c-l**) Bar graphs comparing DMSO controls and samples which showed increased fusion post Yoda1 treatment (red bars) in EDL (left, dark grey bars green points) and soleus (right, light grey blue points)-derived myotubes. Data is mean ± SEM from three experiments (n = 3 mice). p values are annotated above graphs showing significance compared to DMSO control conditions at each size bin using 2-tailed unpaired student t-test. one-way ANOVA followed by the Tukey-Kramer post-hoc. Please refer to Figure 6 (**a**) and (**c**) for representative images.

Supplementary Figure 4 - *Piezo1* knockdown reduced f-actin intensity in EDL- and SOL-derived myotubes

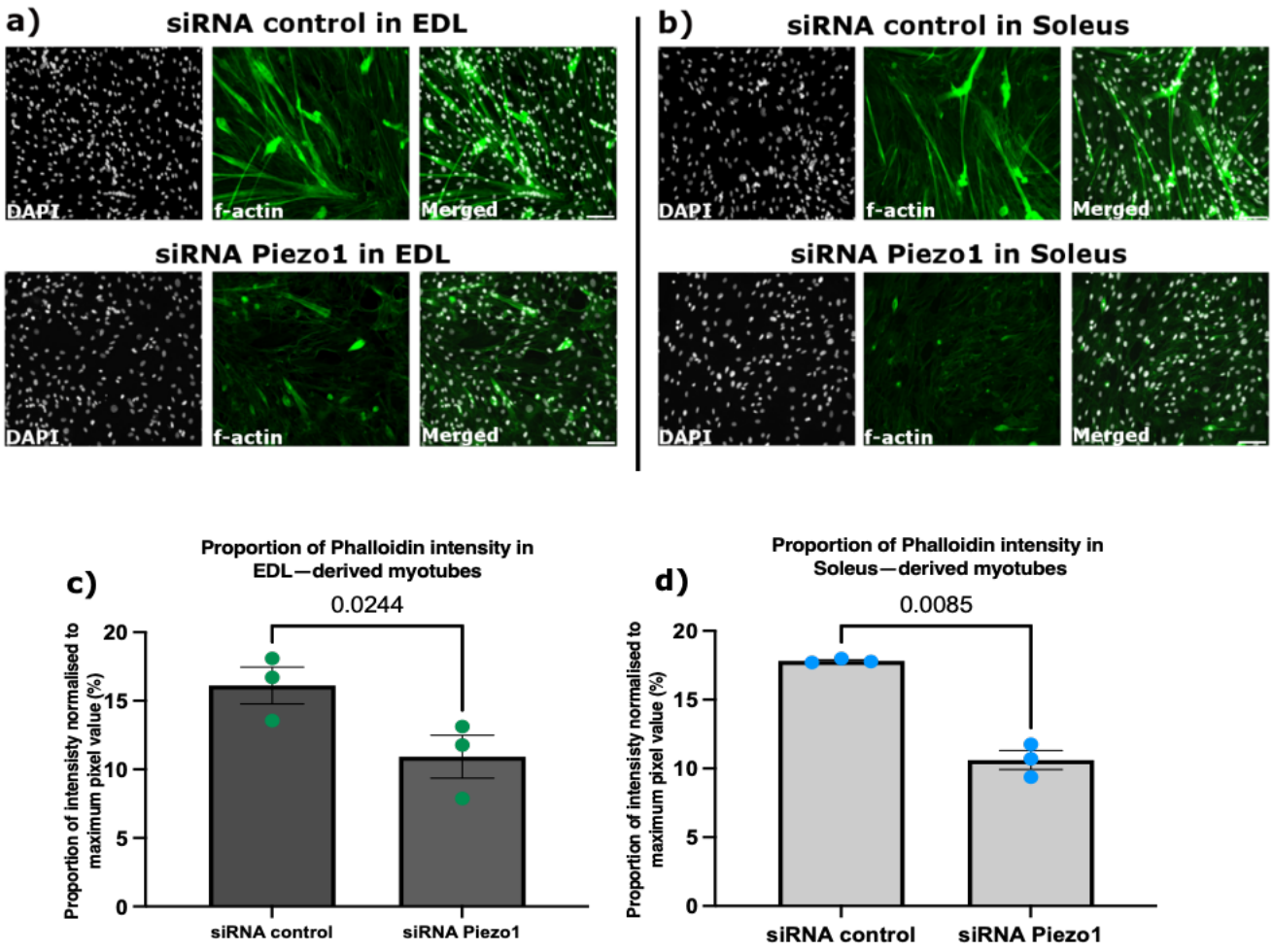

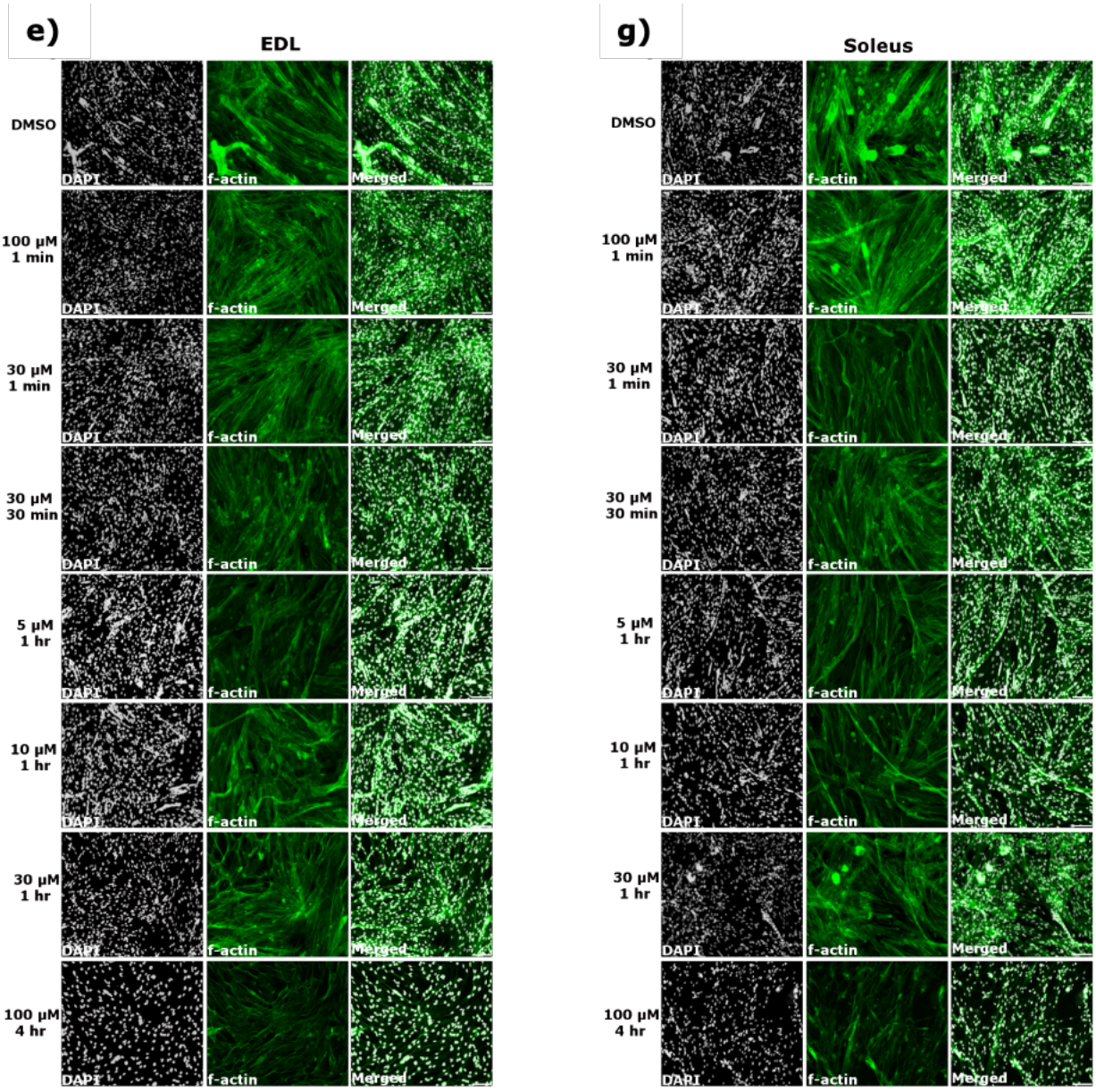

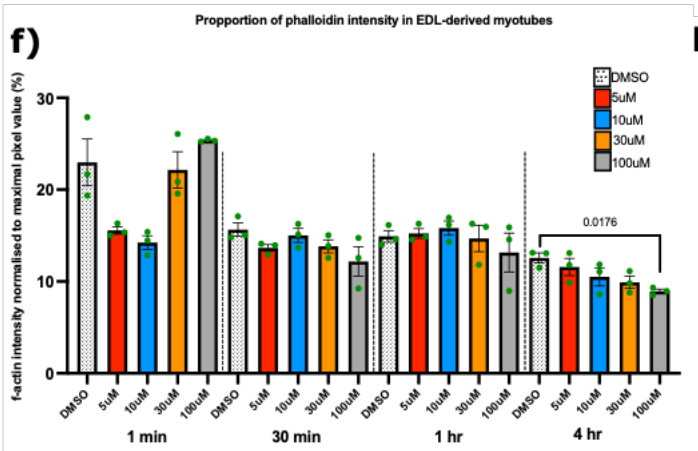

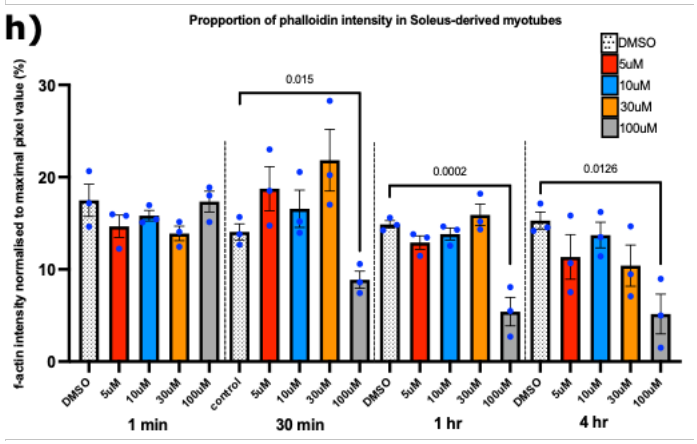

Supplementary Figure 4. *Piezo1* knockdown reduced f-actin intensity in EDL and SOL-derived myotubes. (**a**) and (**b**) Representative images of EDL and soleus muscle-derived myotubes. Early forming myotubes were transfected with 10nM of control-siRNA (siRNA control) or Piezo1-siRNA (siRNA Piezo1). Following overnight incubation, cells were incubated for a further 72 hours. The cytoskeleton protein f-actin was visualised using fluorescently labelled phalloidin (green panels). Nuclei were counterstained with DAPI (black and white panels). (**c**) and (**d**) Overall fluorescence intensity measured by pixel/area in each field of view (six images per conditions) and expressed as percentages relative to the maximum pixel value. Data is mean ± SEM from three experiments (n = 3 mice). p values are annotated above graphs compared to siRNA control conditions using a 2-tailed paired student t-test. (**e-h**) Early forming myotubes were administered with either DMSO (control, white dotted bars) or Yoda1 at the following concentration: 5 μM (red bars), 10 μM (blue bars), 30 μM (orange bars) and 100 μM (grey bars). Myotubes were incubated for 1 min, 30 min, 1 hour and 4 hours. Following incubation period, the medium was exchanged with fresh reduced medium (without agonist) and myotubes were cultured for a further 2 days. (**e**) and (**g**) Representative images at relevant timepoints and concentrations treated with fluorescently labelled phalloidin (green panels) and counterstained with DAPI (black and white panels). Images taken at x20 magnification. Scale bar is 100 μm. Bar graphs display proportion of f-actin intensity in (**f**) EDL and (**h**) soleus derived myotubes from each time point and concentration variables. Values are mean ± SEM. p values are annotated above graphs showing significance compared to DMSO control conditions using one-way ANOVA tests followed by the Tukey-Kramer post-hoc. n = 3 mice.

Supplementary Figure 5 - Different *Piezo1* siRNA targets continue to show decrease in myoblast fusion

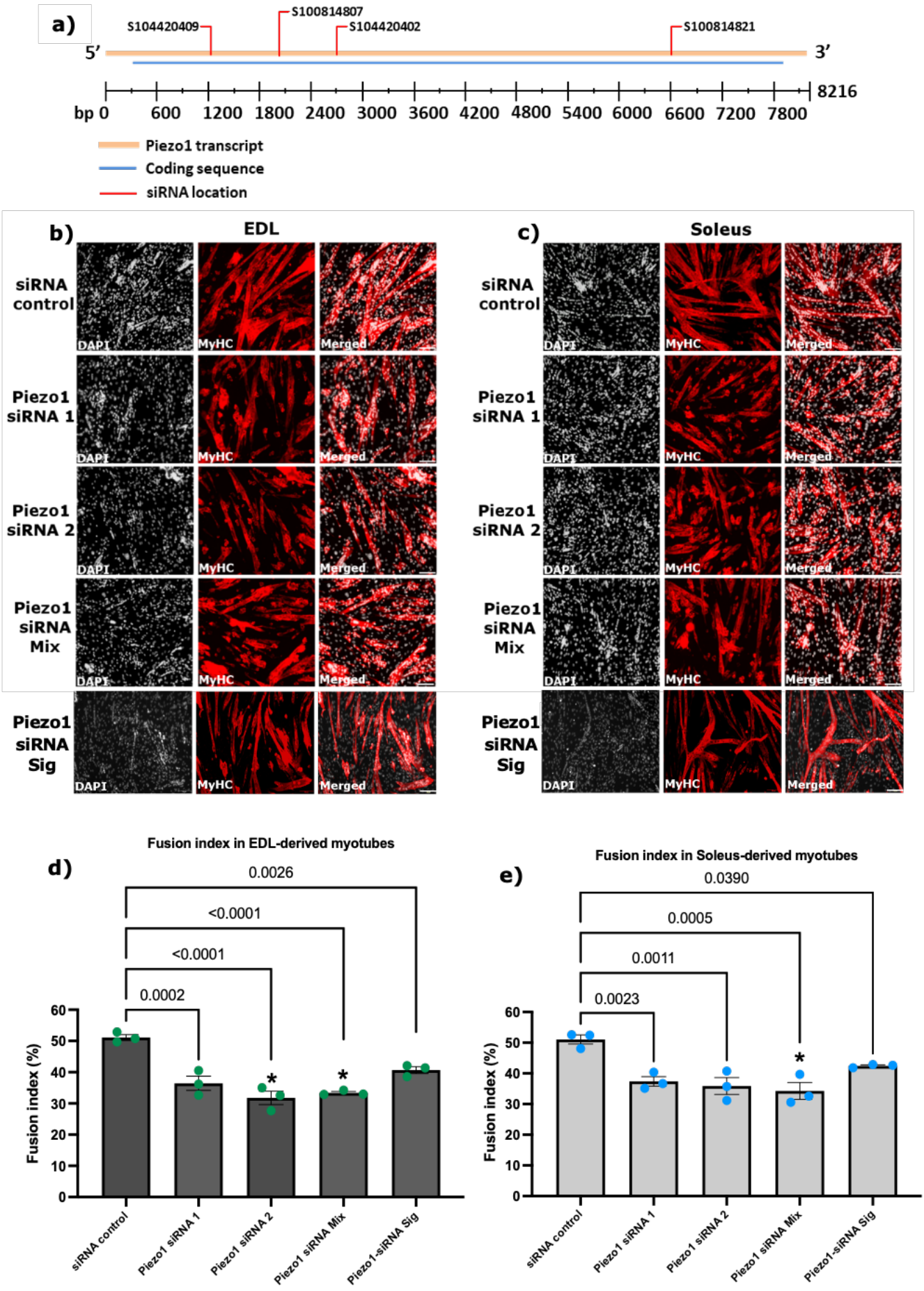

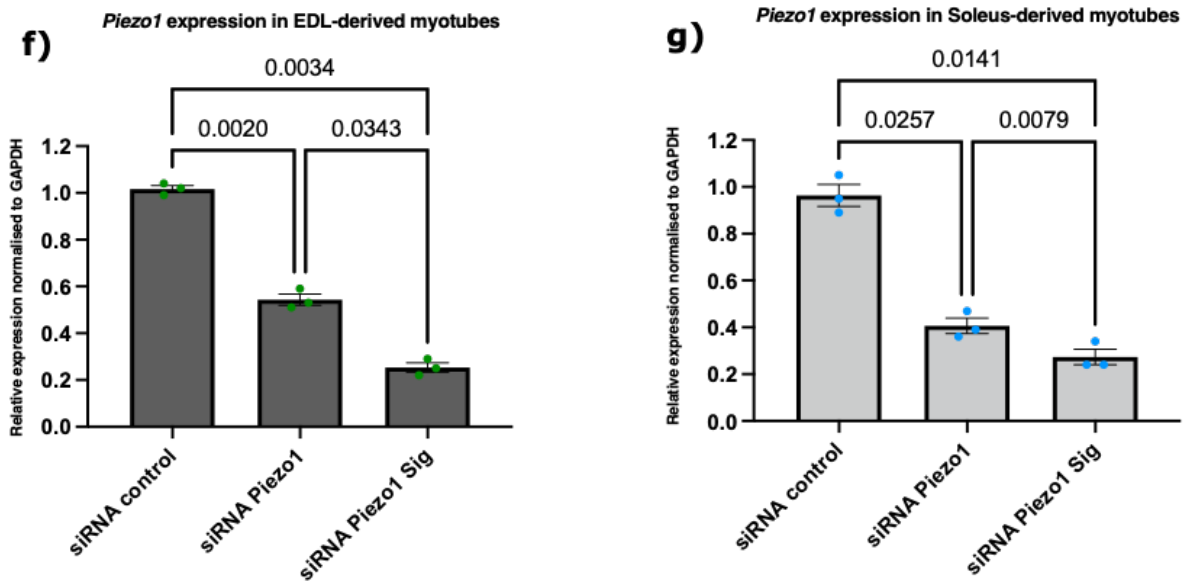

Supplementary figure 5. Different *Piezo1* siRNA targets continue to show decrease in myoblast fusion. (**a**) Location of siRNAs shown in Table 1 on Piezo1 mRNA. Diagram shows Piezo1 mRNA transcript (orange bar), coding sequence (blue bar) and location of each siRNA (red line). bp: base pair. Diagram is adapted from Qiagen (https://geneglobe.qiagen.com/product-groups/flexitube-sirna). (**b**) and (**c**) Representative images of EDL and soleus muscle-derived myotubes, transfected with 10nM of control-siRNA or different siRNAs specific for *Piezo1* (Piezo1-siRNA 1, Piezo1-siRNA 2 and Piezo1-siRNA Sig). A mixture of four different Piezo1-siRNAs from Qiagen (Piezo1-siRNA Mix) including the one in the main text (Table 2) was also used at 10 nM (2.5 nm each). Myoblasts were transfected and incubated overnight; cells were incubated for a further 72 hours in differentiation medium. Cells were immunolabelled for Myosin heavy chain (MyHC) (red panels) and counterstained with DAPI (black and white panels). (**d**) and (**e**) The fusion index was calculated by counting the total number of nuclei within each myotube (more than two nuclei per myotube) and representing this as a percentage relative to the total number nuclei in the image taken. (e) and (f) Relative expression of *Piezo1* in (e) EDL and (f) Soleus derived myotubes transfected with 10nM of siRNA control or siRNA Piezo1 (Qiagen, S104420409) or siRNA Piezo1 Sig. Data is mean ± SEM from three experiments (n = 3 mice). p values are annotated above graphs showing significance compared to siRNA-control conditions using one-way ANOVA followed by the Tukey-Kramer post-hoc. An asterisk (*) denotes significance at $p < 0.05$ compared to Piezo1-siRNA Sig. From table 2, Piezo1 siRNA 1 corresponds to Qiagen, S104420402. Piezo1 siRNA 2 corresponds to Qiagen, S100814807. Piezo1 siRNA Sig corresponds to Sigma: SASI_Mm01_00281158

Supplementary Figure 6 - *Myomaker* is upregulated in response to Piezo1 activation

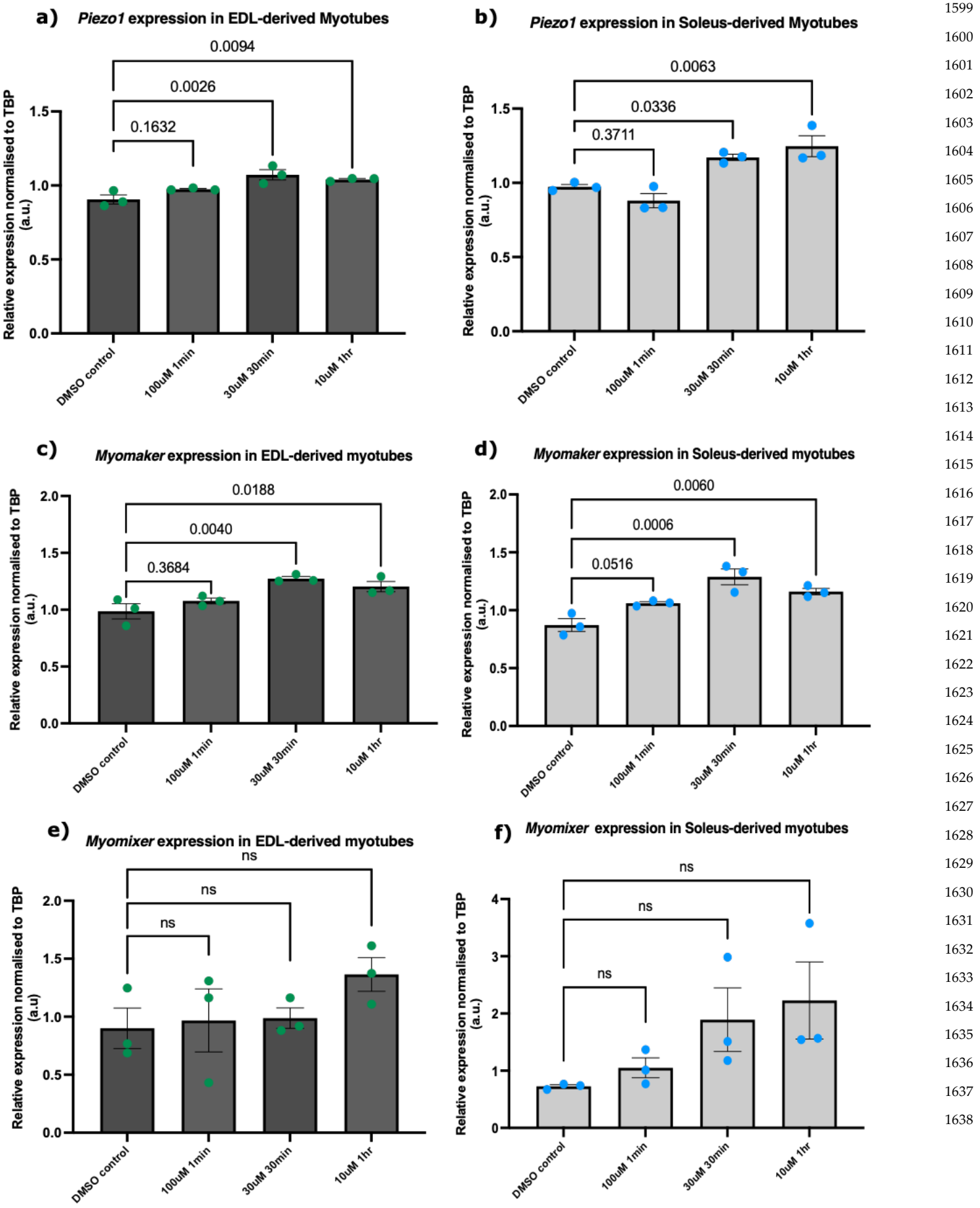

Supplementary figure 6. ***Myomaker*** **is upregulated in response to Piezo1 activation.** Early forming myotubes were subjected to either DMSO or Yoda1 at 100 μM, 30 μM and 10 μM for 1 min, 30 min and 1 hr respectively. Following incubation, medium was exchanged and myotubes were cultured for a further 2 days. Cells were then collected and RT-qPCRs were performed. (**a**) and (**b**) *Piezo1* expression showed significant increase at 30 μM; 30 min and 10 μM; 1 hr in EDL- and soleus-derived myotubes. Similarly, both (**c**) EDL- and (**d**) soleus-derived myotubes showed increased *Myomaker* expression compared DMSO controls. *Myomixer* on the other hand showed no statistically significant change in expression in (**e**) EDL- or (**f**) soleus-derived myotubes. p values are annotated above graphs showing significance (or ns, not significant) compared to DMSO-control conditions using one-way ANOVA followed by the Tukey-Kramer post-hoc. n = 3 mice.